AN ABSTRACT OF THE THESIS OF

Deyan Chen for the degree of Master of Science in Electrical and Computer Engineering presented on March 10, 2016.

Title: PAPR Reduction of Optical OFDM System with Exponential Companding Transform and Zero Padding

Abstract approved: _____

Huaping Liu

Optical wireless communication (OWC) is an alternative to radio frequency (RF) communication with a significantly larger and unregulated spectrum. In OWC systems, optical orthogonal frequency division multiplexing (O-OFDM) with intensity modulation and direct detection (IM/DD) is commonly used. There are two common signal structures in most OWC systems based on IM/DD OFDM. One is called DC-biased optical OFDM (DCO-OFDM) and the other one is called asymmetrically clipped optical OFDM (ACO-OFDM). One drawback of an OFDM signal is its high peak-to-average power ratio (PAPR), which requires the transmitter to operate in a large dynamic range to retain all desirable information. To reduce the PAPR, companding transform has been investigated. Because of the nonlinear operation of companding, a high electrical signal-to-noise ratio (SNR) is required. In this thesis,

a combination of an exponential companding transform and a zero padding scheme is employed on both DCO-OFDM and ACO-OFDM systems to reduce PAPR and the required electrical SNR. Systems that employ quadrature amplitude modulation (QAM) with gray-mapping are simulated. Results have shown that the optimized DCO-OFDM and ACO-OFDM reduced the PAPR by about $7dB$ and $11dB$, respectively, through exponential companding. Meanwhile, the required SNR is decreased by approximately $10dB$ in the optimized DCO-OFDM and by approximately $13dB$ in the optimized ACO-OFDM by using zero padding.

PAPR Reduction of Optical OFDM System with Exponential Companding Transform and Zero Padding

by

Deyan Chen

A THESIS

submitted to

Oregon State University

in partial fulfillment of
the requirements for the
degree of

Master of Science

Presented March 10, 2016
Commencement June 2016

Master of Science thesis of Deyan Chen presented on March 10, 2016.

APPROVED:

Major Professor, representing Electrical and Computer Engineering

---

Director of the School of Electrical Engineering and Computer Science

---

Dean of the Graduate School

I understand that my thesis will become part of the permanent collection of Oregon State University libraries. My signature below authorizes release of my thesis to any reader upon request.

Deyan Chen, Author

ACKNOWLEDGEMENTS

I would like to express my deep gratitude to my major advisor, Prof. Huaping Liu, from Electrical Engineering and Computer Science at Oregon State University, US. His kindness and patience have deeply encouraged me, as well as his earnest and rigorous attitude to the work. His pragmatic advice and continuous support were essential for successful completion of my degree.

My completion of this thesis could not have been accomplished without the support of my friends, Zheqiang Su and Chao Wei. Their patience and selflessness are sincerely appreciated and their suggestions greatly enlightened me. Thanks to my roommate, Tao Lyu, for his encouragement on my work.

Finally, I extend heartfelt thanks to my parents. Their valuable suggestions played an important role in my completion of the thesis. I am very grateful for their deep love, emotional support, and encouragement. Special thanks to my father, Zhiping Chen, for his moderate pressure on my thesis.

TABLE OF CONTENTS

TABLE OF CONTENTS (Continued)

Page

LIST OF FIGURES

LIST OF FIGURES (Continued)

LIST OF TABLES

Chapter 1: INTRODUCTION

As the number of wireless users increases rapidly, the demand for bandwidth in mobile communications is growing fast. The next-generation wireless communication systems will deliver higher capacity to support various broadband wireless services, such as high-definition TV (HDTV), mobile videophones, and high-speed Internet access. By the end of 2015, research shows that the total wireless data traffic has reached 6 exabytes (1 EB = 10^9 GB) per month, resulting in a 97% gap between the traffic demand per device and the available data rate per device in the mobile networks [1, 2]. Using the license-free 60 GHz band has recently been proposed by the Wireless Gigabit Alliance, based on which 7 Gbps short-range wireless links have been established with 7 GHz bandwidth [2]. Consider the large number of wireless devices using high-speed data services, the 60 GHz spectrum will still be insufficient to meet the demand.

Optical wireless communication (OWC) [1,3,4] is one of the promising alternative schemes for addressing the "last mile" bottleneck for emerging broadband wireless access. OWC aims to provide free-space optical (FSO) links over long distances. This can be implemented by employing highly directional laser diodes (LD) as transmitters [5, 6] or for indoor mobile wireless networks by using diffuse light emitting diodes (LEDs) as transmitters [6–9]. In such systems, information is modulated in the optical domain, e.g., light intensity, which restricts the transmitted signal to be real

and positive.

Intensity modulation and direct detection (IM/DD) [2, 10, 11] is widely used for OWC systems. Optical wavelengths in the visible light spectrum range from $380nm$ to $750nm$, whereas wavelengths range from $750nm$ to $2.5um$ [5] in the near infrared (NIR) spectrum. On aggregate, this leads to a total available bandwidth of approximately 670 THz, which is, $10,000$ times larger than the radio frequency (RF) spectrum, as shown in Figure 1.1.

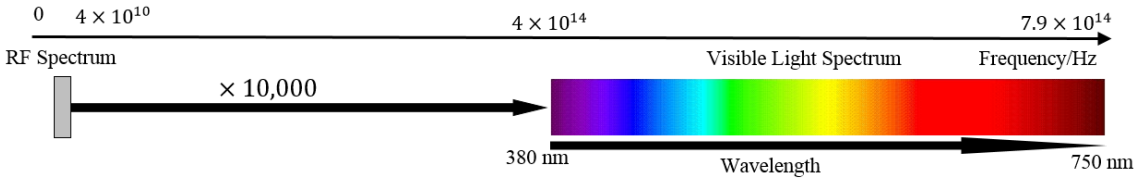

Figure 1.1: Comparison of optical and RF spectrum.

Common transmission schemes for OWC include those developed for RF communications, such as orthogonal frequency division multiplexing (OFDM) [12]. OFDM is a scheme in which a large number of orthogonal, overlapping, narrow band subcarriers, are used to transmit data in parallel. Because of its robustness to narrowband interference and to multi-path fading, OFDM has been used for the high-speed digital communications such as digital audio broadcasting (DAB), digital video broadcasting (DVB), digital High-definition television (HDTV), and asymmetric digital subscriber line (ADSL) [13]. In conventional OFDM systems, the transmitted signals are bipolar and complex. Thus, they are not suitable for OWC systems that employ IM/DD. Therefore, a slight modification to the conventional OFDM signals is needed to ensure Hermitian symmetry of the transmitted signals. Considering the requirements of

OWC IM/DD systems, DC-biased optical OFDM (DCO-OFDM) [14, 15] and asymmetrically clipped optical OFDM (ACO-OFDM) [14,16,17] have been introduced for OFDM. In DCO-OFDM, time-domain signals are DC biased to make sure that most of the OFDM signals are positive (clip all the remaining negative parts, if there are any, at zero level). In ACO-OFDM, odd subcarriers are used to carry information while even subcarriers are set to zero. Constructing the data in this way, all negative parts of the transmitted signal can be clipped at zero and restored from corresponding positive parts at the receiver. However, clipping noise is generated and falls onto even subcarriers.

A drawback of DCO-OFDM and ACO-OFDM is their PAPR [18], resulting from the possibility of individual subcarrier signals adding up coherently. A high PAPR means that the optical source (e.g., LEDs), as well as other nonlinear devices (e.g., power amplifiers (PAs), digital-to-analog converters (DACs)) at the transmitter, must operate in a large dynamic region to accommodate all desirable information. However, devices with a large dynamic range are usually cost-inefficient. In order to reduce the PAPR, researchers are investigating software techniques to enable the nonlinear devices to work within normal dynamic region. Those techniques include selective mapping (SLM) [19–24], partial sequence transmission (PTS) [19, 25–27], and asymmetrical clipping and filtering technique [18, 28, 29], etc. However, these methods either have a high computation complexity, (e.g., SLM and PTS), or introduce a large distortion, (e.g., asymmetrical clipping and filtering technique). Furthermore, as the modulation constellation size and the number of subcarriers increase, the complexity and distortion increase drastically.

Exponential companding transform [30–33] has recently been developed to reduce PAPR. In [31–33], the conventional RF systems implemented PAPR reduction of bipolar OFDM signals modulated by Quadrature Phase-Shift Keying (QPSK) through exponential companding. By transforming the amplitude of original OFDM signals into uniform distribution, exponential companding is able to reduce PAPR effectively for different modulation formats and subcarrier sizes without computation complexity increasing and bandwidth expansion. In [33], exponential companding was firstly introduced into the Visible Light Communication (VLC) systems, in which the OFDM signal is modulated by Binary Phase-Shift Keying (BPSK). In both RF and VLC systems, even though PAPR is significantly reduced, signal is distorted by the nonlinear operation of exponential companding, leading to the still-unsolved problem that a high electrical SNR is required. In [34], zero padding is firstly applied to the ACO-OFDM system for the reduction of the required electrical SNR. By inserting zeros into the transmitted signal, the required SNR is decreased, however, leaving the PAPR problem unsolved.

In this thesis, a combination of the exponential companding and the zero padding scheme is employed in DCO-OFDM and ACO-OFDM systems to reduce the PAPR and the required electrical SNR. By using the proposed scheme, both systems are optimized that the PAPR is reduced through exponential companding, and simultaneously the required electrical SNR is decreased by zero padding. Furthermore, due to the zero padding, no DC bias needed for the transmitted signals in DCO-OFDM, making it more power-efficient. In order to observe the performances of exponentially companded DCO-OFDM and ACO-OFDM without QPSK or BPSK,

both systems are modulated by Quadrature Amplitude Modulation (QAM) with gray mapping, and verified through Monte Carlo simulation. Simulation shows that the optimized DCO-OFDM slightly outperforms the optimized ACO-OFDM with higher bandwidth efficiency in terms of electrical SNR at a target BER of 10^{-4} when the same PAPR reduction is achieved.

The rest of the thesis is organized as follows: **Chapter 2** introduces the background of OWC, including the brief history of OWC, optical OFDM system, IM/DD system. The history and principle of OFDM system are also presented, followed by its mathematical expression and IFFT/FFT implementation. The drawback of the OFDM system, PAPR, will be discussed in this chapter, as well as the derivation of exponential companding transform, which is verified through Monte Carlo simulation in MATLAB.

In **Chapter 3**, the general models of the transmission link in OWC are presented. Section 3.2 introduces the data structure of the conventional DCO-OFDM for OWC based on IM/DD, followed by its power and spectral efficiency analysis, which includes the calculation of DC bias and BER at the receiver. The verification of the conventional DCO-OFDM is simulated through Monte Carlo simulation in the Additive White Gaussian Noise (AWGN) channel at the end of the section, in which the DC bias is set to be twice of the electrical average power of the transmitted signals. Section 3.3 introduces the ACO-OFDM model, including the analysis of clipping noise and the calculation of power and spectral efficiency. The verification of the conventional ACO-OFDM through Monte Carlo simulation in AWGN channel is also given in the section. The last section introduces the principle of the modified

DCO-OFDM and ACO-OFDM models, including the change of required electrical SNR.

In **Chapter 4**, performances of DCO-OFDM and ACO-OFDM modulated by QAM are presented when either exponential companding or zero padding is employed. The feasibility of DCO-OFDM and ACO-OFDM is demonstrated by Monte Carlo simulation. In Section 4.2, performance of the companded DCO-OFDM system is given, followed by the comparison of companded and uncompanded systems. Then zero padding is applied to the uncompanded DCO-OFDM system for the reduction the required electrical SNR. Comparison of the conventional and modified DCO-OFDM without companding is given at the end of the section. In the next section, performance of the companded ACO-OFDM is shown, followed by the comparison between companded and uncompanded ACO-OFDM. A modified model of uncompanded ACO-OFDM is also given. The comparison of conventional and modified ACO-OFDM without companding is presented at the end of the section. In section 4.4, the companded DCO-OFDM is compared with the companded ACO-OFDM without zero padding, in order to show the different performances of exponential companding transform in both systems.

In **Chapter 5**, optimized DCO-OFDM and ACO-OFDM systems are implemented by combining exponential companding and zero padding. Performance of the optimized DCO-OFDM is given in the first section, followed by the comparison of the companded conventional DCO-OFDM and the optimized system. The optimized DCO-OFDM system will be also compared with uncompanded modified system. In the second section, the optimized ACO-OFDM system is given, followed

by the comparison of the optimized system and the companded conventional system. Then, the optimized ACO-OFDM and the uncompanded modified system will be compared. To demonstrate the different performances between DCO-OFDM and ACO-OFDM, comparion of the optimized DCO-OFDM and the optimized ACO-OFDM is discussed in the next section.

Chapter 6 concludes the thesis with the significant implementations of this study. The limitations of the work are discussed. Outlook and future work of this thesis are also presented in this chapter.

Chapter 2: BACKGROUND

2.1 Brief history of OWC

Optical communication is any form of telecommunication that transmits information by means of light. Built by French engineer Claude Chappe in 1792, the earliest form of OWC was called semaphore lines that were able to transmit 196 encoded information symbols. Another application of early OWC was called the heliograph, signaling flashes of sunlight by rotating a mirror or interrupting the beam with a shutter. However, what can be termed as the first optical communication in an unguided channel was the photophone experiment by Alexander Graham Bell in 1880 [33]. The transmitter in his experiment was able to modulate a voice message onto a light signal through vibrating a mirror over a distance of about $200m$, and at the focal point of the receiver, a signal was obtained and demodulated by a crystalline selenium cell.

In the 1960s, OWC changed due to the discovery of the most importantly optical source, the laser. In the early 1960s into the 1970s, some free-space optical (FSO) communication [5] demonstrations were recorded, which included the spectacular transmission of television signal over a $48km$ distance using GaAs LED by MIT Lincoln Laboratory researchers in 1962; an implementation by modulating voice onto an He-Ne laser for transmission over $190km$ between Panamint Ridge and San Gabriel Mountain, USA, was demonstrated in 1963. Around 1970, the first laser link

was built in Japan by Nippon Electric Company (NEC) to solve commercial traffic problems. This link was able to transmit signal over a distance of $14km$ between Yokohama and Tamagawa by employing a full duplex $0.6328um$ He-Ne laser.

As a complementary technology to RF communications, OWC was first proposed as a medium for short-range wireless communication about two decades ago [2]. OWC systems offer a number of unique advantages over RF, such as an abundance of unregulated bandwidth, a secure connectivity, a lower power consumption, immunity to electromagnetic interference, a relatively low cost, and an easy installation. Additionally they require no utilization tariffs, no multipath fading when intensity modulation and direct detection (IM/DD) [11] is used, and they are small, light, and health-friendly.

The first indoor OWC system was reported by Gfeller and Bapst in 1979 [6, 35]. The system employed the infrared (IR) spectrum with a center wavelength of $950nm$ to achieve a data rate of 1 Mbps using on-off keying (OOK) modulation, and implemented the information transmission of an office room through diffuse radiation. In 1996, a data rate of 50 Mbps was achieved by Marsh and Kahn in an indoor diffuse OOK IR system [2,5]. Later in 2000, Carruthers and Kahn implemented a data rate of 70 Mbps and a potential of up to 100 Mbps in a faster diffuse OOK IR system [2,5]. In 2003, a data rate of 400 Mbps was achieved by Tanaka *et al.* in an OOK LED system. By using optical OFDM (O-OFDM), a data rate of 500 Mbps is possible via VLC systems, as reported by Vucic *et al.* [5].

Most practical OWC systems use light-emitting diodes (LEDs) [3, 7–9] or laser diodes (LDs) [4] as transmitters, and PIN photodiodes or avalanche photodiodes

(APDs) as receivers. In 2011, the Institute of Electrical and Electronics Engineers (IEEE) published a standard for VLC, IEEE Std 802.15.7-2011, "IEEE Standard for Local and Metropolitan Area Networks, Part 15.7: Short-Range Wireless Optical Communication Using Visible Light" [2].

2.2 Modulation, transmission and detection in OWC systems

2.2.1 Optical OFDM

As an attractive technology for wireless communications, OFDM offers a high spectral efficiency, a multipath delay spread tolerance, immunity to the frequency selective fading channels, and power efficiency. In the low-cost segment of optical networks such as fiber access and indoor OWC systems [12], the time-domain OFDM signal envelope is applied on a light source (e.g. LEDs) to modulate the optical intensity. For those low-cost approaches, IM/DD is preferred for both wireless and wired OFDM-based optical links. In IM/DD systems, the electric signal is used to directly drive the optical source, which implies that the OFDM signal applied to the optical transmitter must be real and positive. A real-valued time domain signal is obtained by imposing Hermitian symmetry on the OFDM subcarriers. DCO-OFDM and ACO-OFDM are two general types of OFDM techniques tailored for OWC based on IM/DD. In order to make the signals non-negative, DCO-OFDM system is DC biased, while ACO-OFDM system clips the negative signals at zero before transmission.

2.2.2 Intensity modulated/direct detection (IM/DD)

In most OWC systems, IM/DD are commonly used. Figure 2.1 is a model of IM/DD system in which AWGN is added in the electrical domain.

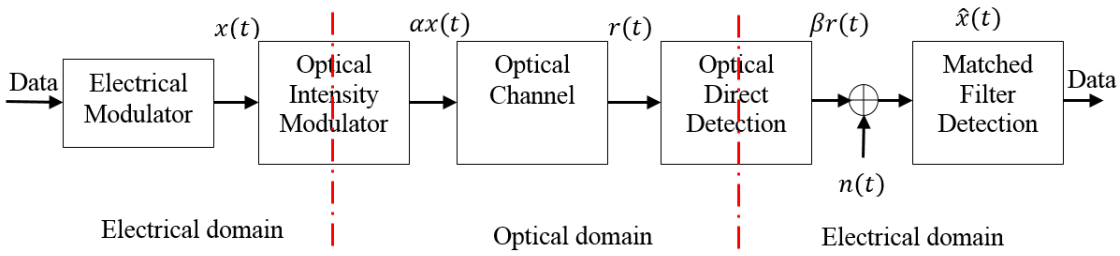

Figure 2.1: Optical wireless system with intensity modulation direct detection.

Data is modulated onto an electrical signal, $x(t)$, which may be represented by either current or voltage. The optical intensity signal that is generated by optical intensity modulator is proportional to $x(t)$, not $x^2(t)$. It means that $x(t)$ can only take positive values, and modulation techniques commonly used in radio communications must be modified for application in OWC systems. Shot noise caused by the ambient signals, which are mainly at DC and can be filtered out, is modeled as AWGN. The received signal can be expressed as:

$$\hat{x}(t) = \beta \times r(t) + n(t) \tag{2.1}$$

where $n(t)$ is AWGN. Data is recovered from $\hat{x}(t)$ by employing a matched filter at the receiver.

2.3 OFDM systems

2.3.1 Brief history of OFDM systems

The concept of transmitting data in parallel and frequency multiplexing was published in the mid-1960's [36], and three decades after which OFDM has been widely used in high speed digital communications. In 1971, Weistein and Ebert introduced the DFT algorithm into OFDM baseband modulation and demodulation, making OFDM technique a more effective processing technology, and avoiding employing lots of subcarrier oscillators [36]. In 1980, Peled and Ruiz inserted a cyclic prefix (CP) in front of the OFDM signal to combat dispersion caused by the channel [5]. In 1985, OFDM was employed in mobile communication by Cimini, and after that OFDM developed rapidly and widely, including its use in Digital Subscriber Line (DSL, 1995) [2], European Telecommunications Standards Institute (ETSI) digital audio (video) broadcasting standard (DAB/DVB, 1995-1997), Wireless Local Area Network standard (802.11ag, Wi-Fi, 1999-2002), Wireless Metropolitan Area Network standard (802.16, WiMax, 2004), and the 4G Long Term Evolution (LTE, 2009) standard.

2.3.2 Principle of OFDM

Inter-symbol interference (ISI) caused by a dispersive channel is a major problem that needs to be considered in the design of wireless communication systems. OFDM is a technique that can relieve ISI efficiently. In OFDM, the data to be transmitted

is spread over a large number of subcarriers, which are modulated at a low rate and made orthogonal to one another by choosing an appropriate frequency spacing between them. The model is illustrated in Figure 2.2.

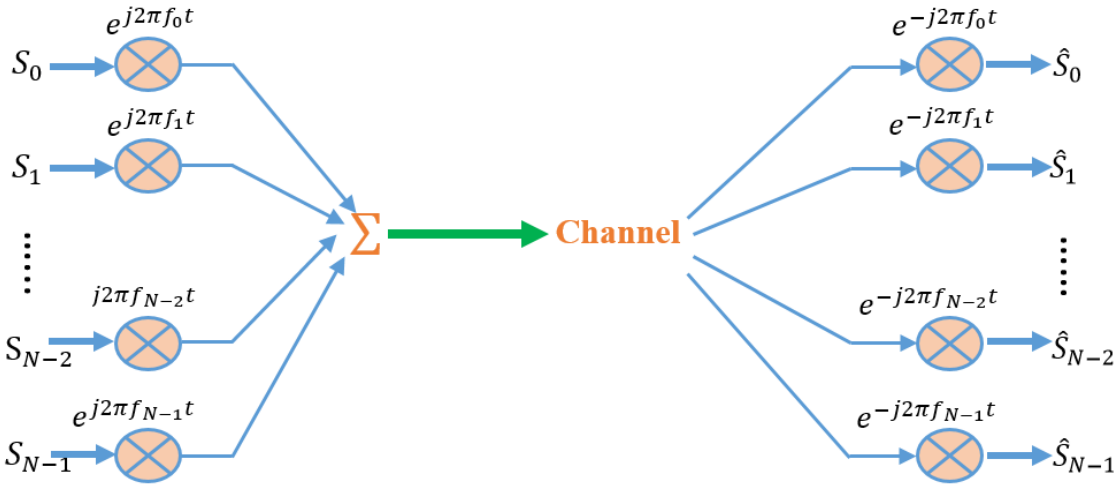

Figure 2.2: Model of OFDM system

In Figure 2.2, $S_k, k = 0, 1, 2, , N-1$, are modulated symbols, each of which is assigned a subcarrier $e^{j2\pi f_k t}$ before parallel-to-series conversion. By providing an inverse subcarrier at the receiver, corresponding symbols can be recovered.

Mathematically, a time-domain OFDM signal can be expressed as:

$$s(t) = \sum_{i=-\infty}^{+\infty} \sum_{k=0}^{N-1} z_{ki} s_k (t - i \times T_s) \tag{2.2}$$

where

$$s_k = \Pi(t) e^{j2\pi f_k t}$$

z_{ki} : the ith information symbol on the kth subcarrier

s_k : the waveform for the kth subcarrier

N : the number of subcarriers

f_k : the frequency of the subcarrier

T_s : the symbol period

$\Pi(t)$: the pulse shaping function, given as

$$\Pi(t) = \begin{cases} 1, & 0 < t < T_s \\ 0, & \text{otherwise.} \end{cases}$$

Using a filter or correlator as a detector that matches the data-carried subcarrier, the detected information symbol, $z_{ki}^{'}$, can be obtained as:

$$z_{ki}^{'} = \int_0^{T_s} y(t - iT_s) s_k^* dt = \frac{1}{T_s} \int_0^{T_s} y(t - iT_s) e^{-j2\pi f_k t} dt \tag{2.3}$$

where $y(t)$ is the received time-domain symbols.

In the classical multi-carrier modulation (MCM), the transmitted signals are separated by a guard interval (GI) to avoid ISI, leading to bandwidth expansion, as shown in Figure 2.3 below.

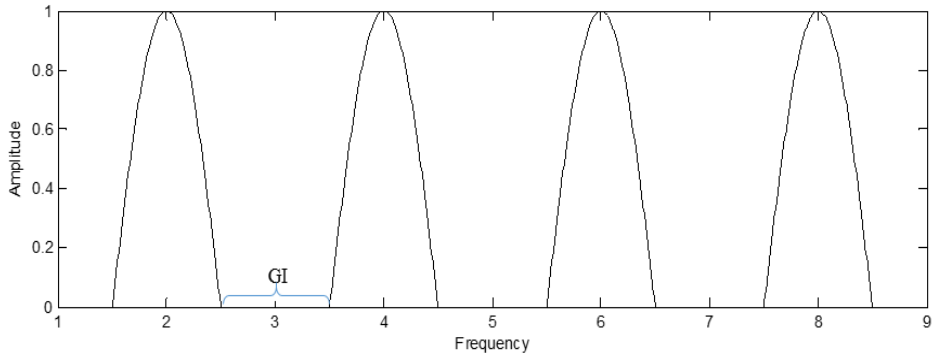

Figure 2.3: MCM signals in the frequency domain.

Compared to the classical MCM, OFDM is a more spectral-efficient scheme that transmits signals in a overlapping format, as illustrated in Figure 2.4:

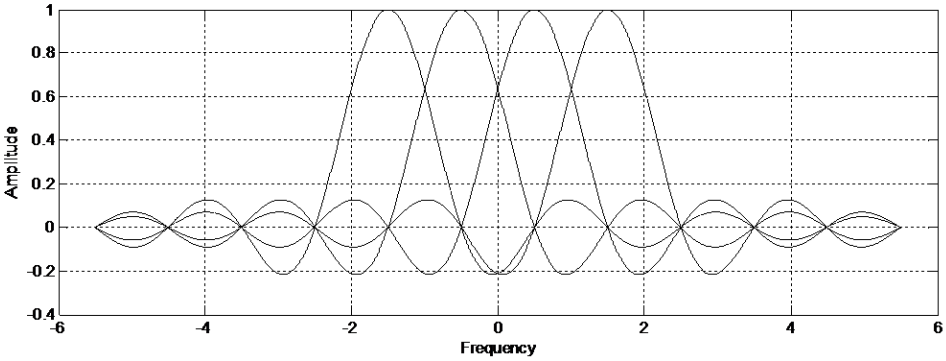

Figure 2.4: OFDM signals in the frequency domain.

The orthogonality between any two subcarriers can be guaranteed by ensuring that

the following correlation equals zero:

$$\begin{aligned}
\xi_{ij} &= \frac{1}{T_s}\int_0^{T_s} s_i s_j^* dt = \frac{1}{T_s}\int_0^{T_s} e^{j2\pi f_i t} e^{-j2\pi f_j t} dt = \frac{1}{T_s}\int_0^{T_s} e^{j2\pi(f_i-f_j)t} dt \\
&= \frac{1}{j2\pi(f_i-f_j)T_s} e^{j2\pi(f_i-f_j)t}|_0^{T_s} = \frac{1}{j2\pi(f_i-f_j)T_s}(e^{j2\pi(f_i-f_j)T_s}-1) \\
&= \frac{1}{j2\pi(f_i-f_j)T_s}(e^{j2\pi(f_i-f_j)T_s} - e^{j\pi(f_i-f_j)T_s - j\pi(f_i-f_j)T_s}) \\
&= e^{j\pi(f_i-f_j)T_s}\frac{\sin(\pi(f_i-f_j)T_s)}{\pi(f_i-f_j)T_s}. \qquad (2.4)
\end{aligned}$$

If

$$f_i - f_j = k\frac{1}{T_s} \qquad (2.5)$$

is satisfied, then any two subcarriers are orthogonal to each other. With their frequencies spaced at integer multiples of the inverse of the symbol rate, the information carried by the orthogonal subcarriers can be recovered with the matched filter as expressed in Eq. (2.4) without inter-carrier interference (ICI). Figure 2.5 and Figure 2.6 illustrate the OFDM signal transmission in the frequency domain and time domain, respectively.

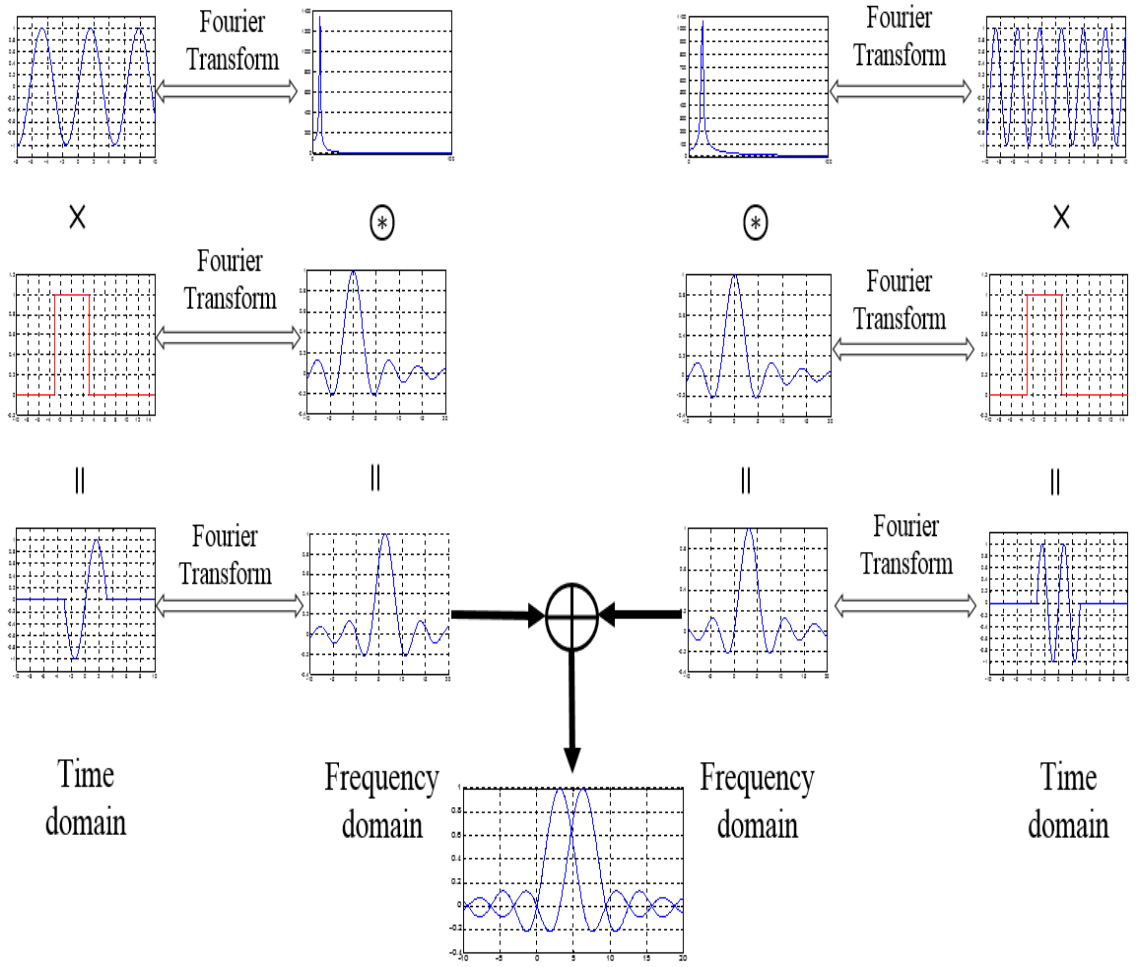

Figure 2.5: Frequency domain OFDM.

At the receiver, the transmitted signals will be restored by sampling at the Nyquist rate.

In the time domain, information symbols, $a_1, a_2, \ldots, a_k$, are modulated onto sinusoidal waveforms, e.g., $sin(t)$ or $cos(t)$, with different frequencies, which are then summed up for transmission through the channel, as shown in Figure 2.6:

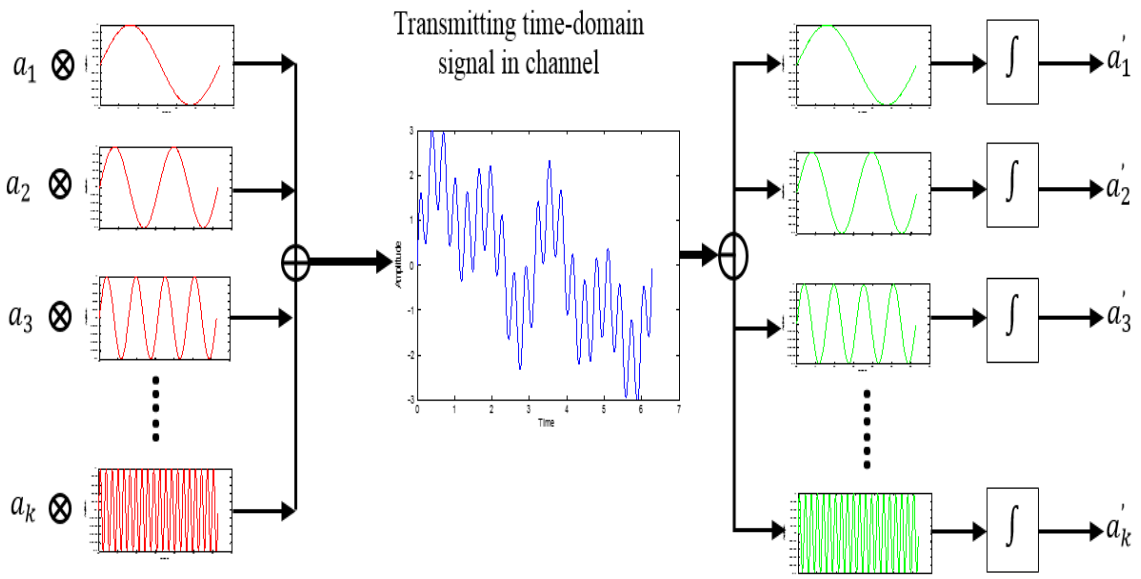

Figure 2.6: OFDM signaling in the time domian.

The OFDM demodulation process as shown in Figure 2.6 can also be expressed mathematically as:

$$\begin{aligned} f(t) &= a_1 \cdot \sin(2\pi\Delta ft) + a_2 \cdot \sin(2\pi\Delta ft) + \ldots + a_k \cdot \sin(2\pi\Delta ft) \ldots \\ &+ b_1 \cdot \cos(2\pi\Delta ft) + b_2 \cdot \cos(2\pi\Delta ft) + \ldots + b_k \cdot \cos(2\pi\Delta ft) \\ &= \sum_{k=-\infty}^{\infty} a_k \sin(2\pi\Delta fkt) + \sum_{k=-\infty}^{\infty} b_k cos(2\pi\Delta fkt) \\ &= \sum_{k=-\infty}^{\infty} F_k e^{j2\pi\Delta fkt} \end{aligned} \tag{2.6}$$

where

$$F_k = \frac{1}{T} \int_{-\frac{T}{2}}^{\frac{T}{2}} f(t) e^{-j2\pi\Delta fkt} dt.$$

An efficient way to implement Eq. (2.6) in most practical OFDM systems is to employ the fast Fourier transform (FFT).

2.3.3 IFFT/FFT implementation of OFDM

In most OFDM systems, an OFDM signal can be expressed by discrete Fourier transform(DFT)/inverse DFT, which is computed efficiently by using the fast Fourier transform (FFT)/inverse FFT algorithm invented by J. W. Cooley and John Tukey in 1965 [33]. The IDFT/DFT can be expressed as:

IDFT:

$$x_m = \frac{1}{\sqrt{N}} \sum_{k=0}^{N-1} X_k e^{\frac{j2\pi km}{N}}, \quad m = 0, 1, \ldots, N-1. \tag{2.7}$$

DFT:

$$X_k = \frac{1}{\sqrt{N}} \sum_{m=0}^{N-1} x_m e^{-\frac{j2\pi km}{N}}, \quad , k = 0, 1, \ldots, N-1. \tag{2.8}$$

Note that the forward and inverse discrete Fourier transform may be defined differently in different publications. In order to maintain the orthogonality of subcarriers in a dispersive channel, one of the challenges of OFDM signals is to mitigate the effects of channel dispersion. One of the enabling techniques is the insertion of a CP. The CP extends the OFDM symbol by copying the last segment of the symbol into its head side, leading to the OFDM symbol be cyclically extended into the guard interval. Figure 2.7 illustrates the mitigation of dispersion by the insertion of CP. Consider two consecutive OFDM signals, A and B, that undergo a dispersive channel with a delay of t_d. Because of the channel delay, the first few samples of Symbol A will be distorted by Symbol B at the receiver:

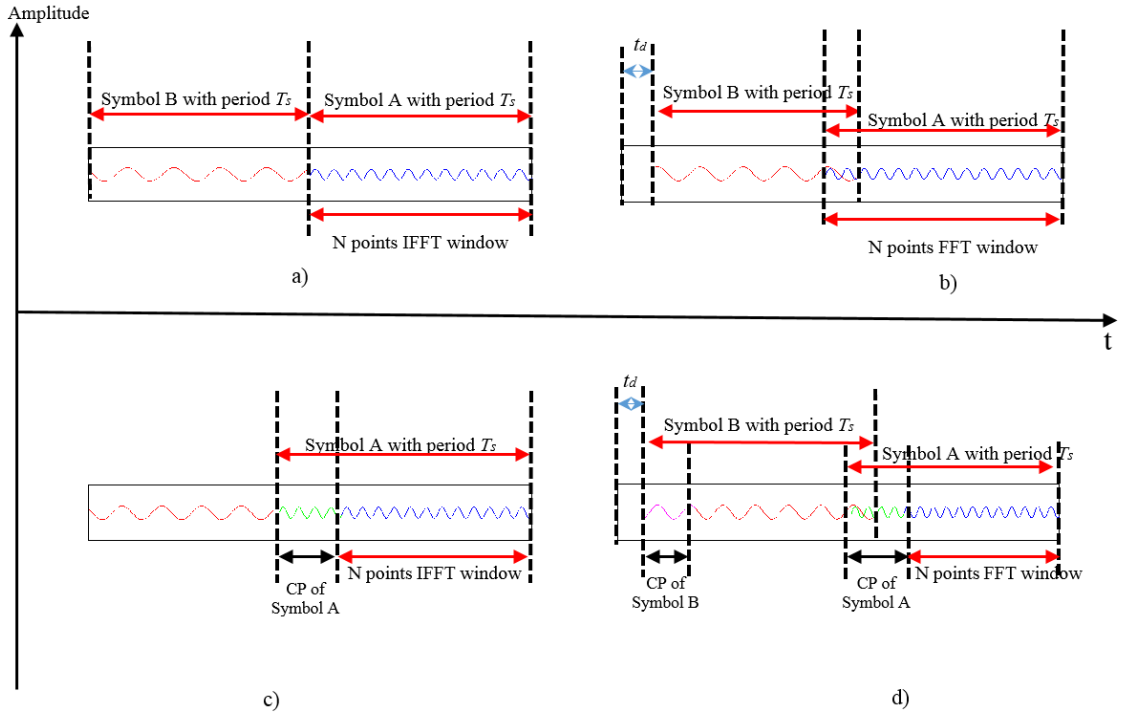

Figure 2.7: OFDM signals in a channel with delay spread of t_d. a) without cyclic prefix at the transmitter. b) without cyclic prefix at the receiver. c) with cyclic prefix at the transmitter. d) with cyclic prefix at the receiver.

With the CP insertion, which is longer than the maximum delay of the channel, Symbol B extends into the CP of Symbol A without affecting the desirable data portion of Symbol A. In this way, the ISI problem is solved, and the orthogonality of subcarriers is also maintained simultaneously. The overall OFDM system block diagram, therefore, can be illustrated as:

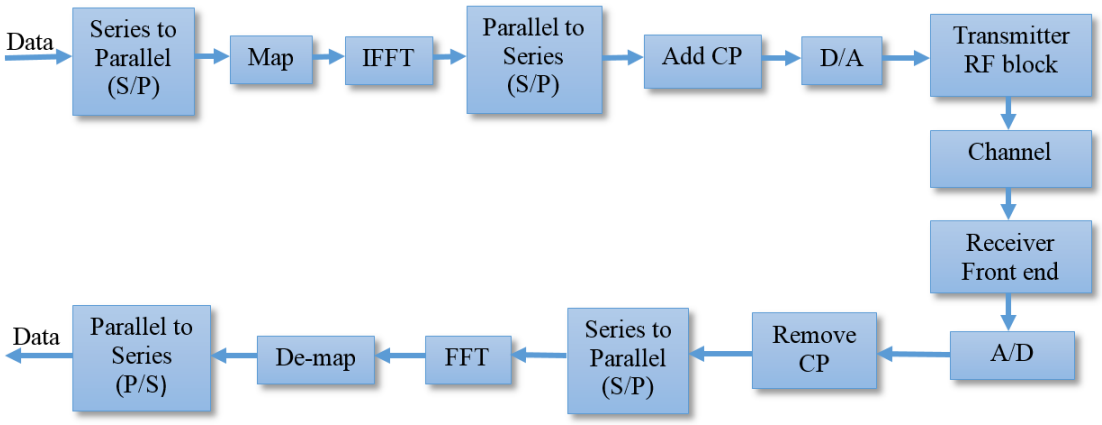

Figure 2.8: OFDM system block diagram.

2.3.4 PAPR of OFDM

According to Eq. (2.7), OFDM signals have a high peak-to-average power ratio (PAPR) due to the probability of individual signal adding up. The PAPR, refering to the ratio of maximum power and average power of the OFDM signal, is commonly defined as [18]:

$$PAPR(dB) = \frac{P_{peak}}{P_{average}} = 10\log_{10}\frac{\max\limits_{0<m<N-1}[|x_m|^2]}{E[|x_m|^2]} \tag{2.9}$$

where x_m are the time-domain OFDM signals and E[·] denotes statistical expectation. In particular, the OFDM signal has a theoretical maximum value that equals to:

$$PAPR_{max} = 10\log_{10}(N)(dB) \tag{2.10}$$

where N is the number of subcarriers.

According to the central limit theorem (CLT), when the number of subcarriers is large (e.g. $N > 64$), the real and imaginary parts of x_m become Gaussian-distributed, leading to a Rayleigh distribution for the amplitude of OFDM signal.

The complementary cumulative distribution function (CCDF) is a commonly used parameter to measure the efficiency of PAPR reduction techniques in practical systems:

$$P(PAPR \leq z) = 1 - (1 - e^z)^N \tag{2.11}$$

where z is a selected threshold. CCDF denotes the probability that the PAPR of an OFDM symbol sequence is greater than a certain threshold. By comparing the CCDF of various PAPR-reducing methods, the performance of new methods can be easily analyzed.

2.4 Exponential companding algorithm

The purpose of exponential companding [31, 32] is to transform the statistics of the signal amplitudes into a uniform distribution and therefore to reduce the PAPR. Considering the signal implemented by IDFT given by:

$$s_m = \frac{1}{\sqrt{N}} \sum_{k=0}^{N-1} S_k e^{\frac{j2\pi km}{N}}.$$

According to the CLT, when N is large (e.g. $N \geq 64$), the real and imaginary parts of s_m are independent and identically distributed (i.i.d.) Gaussian random

variables with a zero mean and variance $\sigma^2 = E[|S_k|^2]/2$. Then, the Rayleigh-distributed amplitude of OFDM signal, s_m, is:

$$|s_m| = \sqrt{Re^2\{s_m\} + Im^2\{s_m\}}. \tag{2.12}$$

The CDF of the amplitude can be expressed as:

$$F_{|s_m|}(z) = P(|s_m| \leq z) = \int_0^z \frac{2y}{\sigma^2} e^{-\frac{y^2}{\sigma^2}} dy = 1 - e^{-\frac{z^2}{\sigma^2}}, \qquad z \geq 0. \tag{2.13}$$

Note that $f(z)$ is a monotonically increasing companding function. Let x_m be the companded output signal, that is,

$$x_m = f(z), z = s_m.$$

To derive the companding function $f(z)$, let $|x_m|^d$ be the dth power of the companded amplitude with a uniform distribution in the interval $[0, \alpha]$, where the exponent d is called the degree of exponential companding transform. Then the CDF of $|x_m|^d$ is given by:

$$F_{|x_m|^d}(z) = \frac{z}{\alpha}, \qquad 0 \leq z \leq \alpha \tag{2.14}$$

and the CDF of the companded amplitude $|x_m|$ is:

$$\begin{aligned} F_{|x_m|}(z) &= P(|x_m| \leq z) \\ &= P(|x_m|^d \leq z^d) \\ &= \frac{z^d}{\alpha}, \qquad 0 \leq z \leq \sqrt[d]{\alpha} \end{aligned} \tag{2.15}$$

and therefore the inverse function, $F^{-1}_{|x_m|}(z)$, can be computed as:

$$F^{-1}_{|x_m|}(z) = \sqrt[d]{\alpha z}, \qquad 0 \le z \le 1.$$

Then we have

$$\begin{aligned} F_{|s_m|}(z) &= P(|s_m| \le z) \\ &= P\big(f(|s_m|) \le f(z)\big) \\ &= F_{|x_m|}\big(f(z)\big), \qquad 0 \le z \le f^{-1}(\sqrt[d]{\alpha}). \end{aligned} \tag{2.16}$$

Switching $F_{|s_m|}(z)$ and $f(z)$, and computing $F^{-1}_{|x_m|}$, we can obtain the companding function $f(z)$ as:

$$\begin{aligned} f(z) &= \text{sign}(z) F^{-1}_{|x_m|}\big(F_{|s_m|}(z)\big) \\ &= \text{sign}(z) \sqrt[d]{\alpha \left[1 - e^{-\frac{z^2}{\sigma^2}}\right]} \end{aligned} \tag{2.17}$$

where sign$(\cdot)$ is the sign function. The positive constant α determines the average power of companded signals. To maintain the input and output signals at the same average power level, α can be determined as:

$$\alpha = \left(\frac{E[|s_m|^2]}{E[\sqrt[d]{[1 - e^{-\frac{|s_m|^2}{\sigma^2}}]^2}]} \right)^{\frac{d}{2}}. \tag{2.18}$$

To recover the received companded signals at the receiver, the inverse function, $f^{-1}(z)$, used in the decompanding process, is given by:

$$f^{-1}(z) = \text{sign}(z) \sqrt{-\sigma^2 \log_e \left(1 - \frac{z^d}{\alpha}\right)}. \tag{2.19}$$

When $d \geq 2$, the exponential companding function is able to compress large signals and expand small signals efficiently at the same time.

2.4.1 Verification of exponential companding through Monte Carlo simulation

To verify the capability of exponential companding transform in reducing PAPR, a baseband DCO-OFDM system shown in Figure 2.9 is considered with the number of subcarriers $N = 64$. For simplicity, no DC bias and CP are added to the transmitted signals. The randomly generated input data are modulated by 64-quadrature amplitude modulation (64-QAM) with gray mapping. Figure 2.9 a) compares the waveforms of original and the companded OFDM signals with $d = 6$; Figure 2.9 b) shows the PAPR reduction of the system.

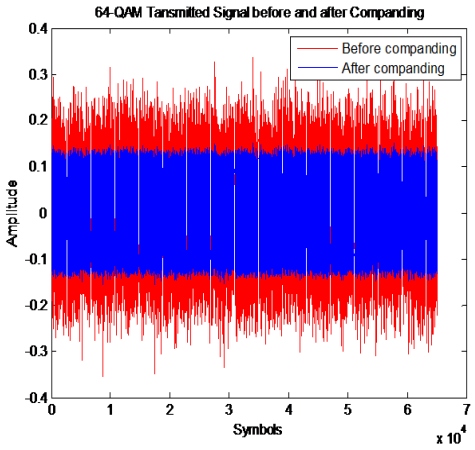

(a) Waveform of companded and uncompanded OFDM signals

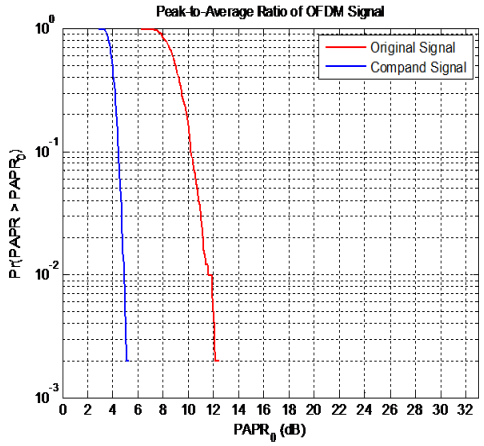

(b) CCDF of the original and companded OFDM signals.

Figure 2.9: Real-value output of OFDM systems with exponential companding method.

Figure 2.9 shows that the PAPR is significantly reduced due to companding. The distribution of the original OFDM signals is transformed to uniform-like distribution, leading to a large reduction of PAPR.

2.5 Summery

In this chapter, OWC based on IM/DD OFDM is presented. The principle of OFDM systems is in time and frequency domains is described, followed by its IFFT/FFT implementation. A drawback of an OFDM system is its high PAPR. Exponential companding transform is derived to reduce the PAPR and its effect are verified through Monte Carlo simulation in a DCO-OFDM system.

Chapter 3: Modulation Techniques for VLC

3.1 Introduction

In OWC based on IM/DD OFDM systems, real signals are obtained by constructing the input, $\mathbf{X}$, of an IFFT block with Hermitian symmetry at the expense of half spectral-efficiency. Below is an example:

$$\mathbf{X} = [X_0, X_1, X_2, \ldots, X_{\frac{N}{2}-1}, X_{\frac{N}{2}}, X^*_{\frac{N}{2}-1}, \ldots, X^*_2, X^*_1, X^*_0].$$

In order to further make the signal non-negative, two common techniques are used in OWC: DC-biased optical OFDM (DCO-OFDM) and asymmetrically clipped optical OFDM (ACO-OFDM). The modified optical OFDM systems can be illustrated as Figure 3.1:

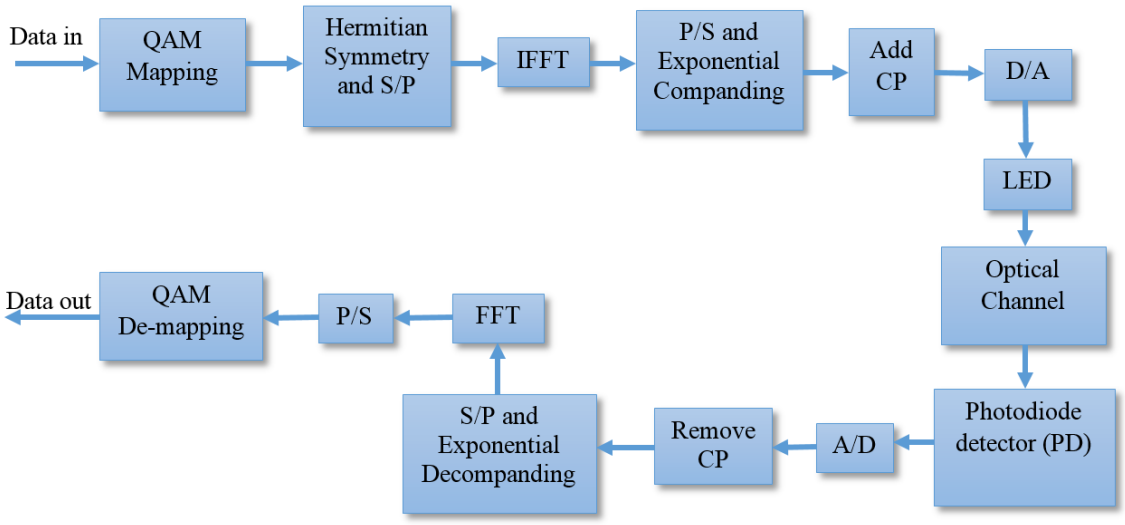

Figure 3.1: Block diagram of optical OFDM systems.

3.2 DCO-OFDM system model

3.2.1 DCO-OFDM

DCO-OFDM system is a commonly used technique in OWC based on IM/DD OFDM systems. To generate real signals, Hermitian symmetry is imposed on the modulated signals before transmission. Further, a DC bias is added to the transmitted signal (clip the rest negative parts, if there are any, at zero) to make it non-negative. The input signal of DCO-OFDM with Hermitian symmetry can be expressed as:

$$\mathbf{S} = [S_0, S_1, S_2, \ldots, S_{\frac{N}{2}-1}, S_{\frac{N}{2}}, S^*_{\frac{N}{2}-1}, \ldots, S^*_2, S^*_1, S^*_0].$$

In addition, the two components S_0 and $S_{N/2}$ are set to zero, that is, $S_0 = S_{N/2} = 0$, to hold the Hermitian symmetry condition. The nth time-domain output of IDFT, s_n, is given by:

$$s_n = \frac{1}{\sqrt{N}} \sum_{k=0}^{N-1} S_k e^{\frac{j2\pi kn}{N}}, \qquad n = 0, 1, \ldots, N-1$$

where N is the number of OFDM subcarriers and S_k is the kth subcarrier of signal $\mathbf{S}$. Due to the Hermitian symmetry, the number of desired symbols that DCO-OFDM is able to transmit is $\frac{N}{2} - 1$.

3.2.2 Spectral and power analysis of DCO-OFDM

To analyze the spectral-efficiency of DCO-OFDM systems, let $G_B = \frac{\frac{N}{2}-1}{N+N_{cp}}$ be the bandwidth utilization factor where N_{cp} is the number of samples of the CP and $B = \frac{1}{T}$ be the double-sided bandwith of the DCO-OFDM signals. Then, the symbol rate can be computed as:

$$\begin{aligned} R_s^{DCO} &= \log_2(M) G_B B \\ &= \log_2(M) \times \frac{\frac{N}{2}-1}{N+N_{cp}} \times \frac{1}{T} \\ &= \frac{N-2}{2(N+N_{cp})T} \log_2(M), \quad \text{bits/s} \end{aligned} \tag{3.1}$$

where M is the modulation order. Due to the Hermitian symmetry of the transmitted signal, the resulting spectral-efficiency is:

$$\begin{aligned} \eta_{DCO} &= \frac{R_s^{DCO}}{B} \\ &= \frac{\log_2(M)(N-2)}{2(N+N_{cp})}, \quad \text{bits/s/Hz.} \end{aligned} \tag{3.2}$$

The QAM signal S_k can be expressed as:

$$S_k = a_k + b_k \tag{3.3}$$

where a_k and b_k are the real and imaginary parts of S_k, respectively. Furthermore, when the number of subcarriers is large (e.g., $N > 64$), a_k and b_k can be approximated as having a Gaussian distribution with a zero mean and variance σ^2 [11]:

$$E[a_k] = E[b_k] = 0$$
$$\sigma^2 = E[a_k^2] - E^2[a_k] = E[a_k^2] = E[b_k^2] - E^2[b_k] = E[b_k^2]$$

let $P_{s(elec)}$ denote the average electrical power per symbol. Then:

$$P_{s(elec)} = 2\sigma^2 = E[a_k^2] + E[b_k^2]$$
$$E[a_k^2] = E[b_k^2] = \tfrac{P_{s(elec)}}{2}, \qquad k \neq 0, \tfrac{N}{2}.$$

Thus, the mean of the time domain signal s_n is given by:

$$E[s_n] = E\left[\frac{1}{\sqrt{N}} \sum_{k=0}^{N-1} S_k e^{\frac{j2\pi kn}{N}}\right] = \frac{1}{\sqrt{N}} \sum_{k=0}^{N-1} E[S_k] e^{\frac{j2\pi kn}{N}} = 0.$$

Similarly, the average power $\sigma_{s_n}^2$ can be calculated as:

$$\begin{aligned}\sigma_{s_n}^2 &= E[s_n^2] = \frac{1}{N}\sum_{k=0}^{N-1}\sum_{l=0}^{N-1} E[S_k S_l] e^{\frac{j2\pi(k+l)n}{N}} \\ &= \frac{1}{N}\sum_{\substack{k=1 \\ k\neq\frac{N}{2}}}^{N-1} P_{s(elec)} e^{\frac{j2\pi(k+(N-k))n}{N}} = (1-\frac{2}{N})P_{s(elec)}. \end{aligned} \tag{3.4}$$

The factor $\frac{2}{N}$ is due to the fact that the two subcarriers, the 0th and $\frac{N}{2}$th subcarriers, are set to zero. The DC bias can be determined by the standard deviation of s_k [8]. Let D_{DC} denote the DC bias. Then we have:

$$D_{DC} = \mu\sqrt{\sigma^2} \tag{3.5}$$

where μ is a constant. Let s_0 be the DC biased signal expressed as:

$$s_0 = s_n + D_{DC}.$$

The DC bias in dB, $D_{DC}(dB)$, can be computed as:

$$D_{DC}(dB) = 10\log_{10}\left[\frac{E[\{s_0\}^2]}{E[\{s_n\}^2]}\right] = 10\log_{10}(\mu^2+1).$$

In the DCO-OFDM system, the optical power of the OFDM symbol, $P_{s(opt)}$, equals to the DC bias, i.e., $P_{s(opt)} = D_{DC}$, for the reason that the useful alternating current (AC) signal power is reduced by the DC bias for a fixed total signal power. Therefore, the relationship between electrical power, $P_{s(elec)}$, and optical

power, $P_{s(opt)}$, can be expressed as [6]:

$$P_{s(elec)} = \frac{\sigma^2 + D_{DC}^2}{D_{DC}^2} P_{s(opt)}^2. \tag{3.6}$$

According to the CLT, the OFDM signals follow a Gaussian distribution with a zero mean and a variance σ^2 when the number of subcarriers is large (e.g., $N > 64$). The probability that at any given time instant the ensemble average of $\mathbf{S}$ equals z is given by:

$$p(\mathbf{S} = z) = \frac{1}{\sqrt{2\pi\sigma^2}} e^{-\frac{z^2}{2\sigma^2}}. \tag{3.7}$$

Therefore, the BER of the DCO-OFDM system using M-QAM can be calculated as:

$$BER = \frac{2(\sqrt{M}-1)}{\sqrt{M}\log_2(M)} \text{erfc}\left(\sqrt{\frac{3E_s/N_0}{2(M-1)}}\right). \tag{3.8}$$

3.2.3 Simulated BER of DCO-OFDM

The BER performance of DCO-OFDM system is simulated. The simulation is assumed that no channel fading and CP adding, ideal synchronization between transmitter and receiver front-ends, and noise is modulated by AWGN. The added DC bias is set to be twice the average power of OFDM signals and the left negative values are clipped at zero level. The size of OFDM signal frame, N, is 130, among which 64 symbols are desirable symbols that are modulated by M-QAM. The number of total transmitted symbols is 500 with a given E_b/N_0 ranges from $-9dB$ to $35dB$. The power of the transmitted signals is normalized to unity. The simulation curve

is bounded by the conventional OFDM RF system, as shown in Figure 3.2.

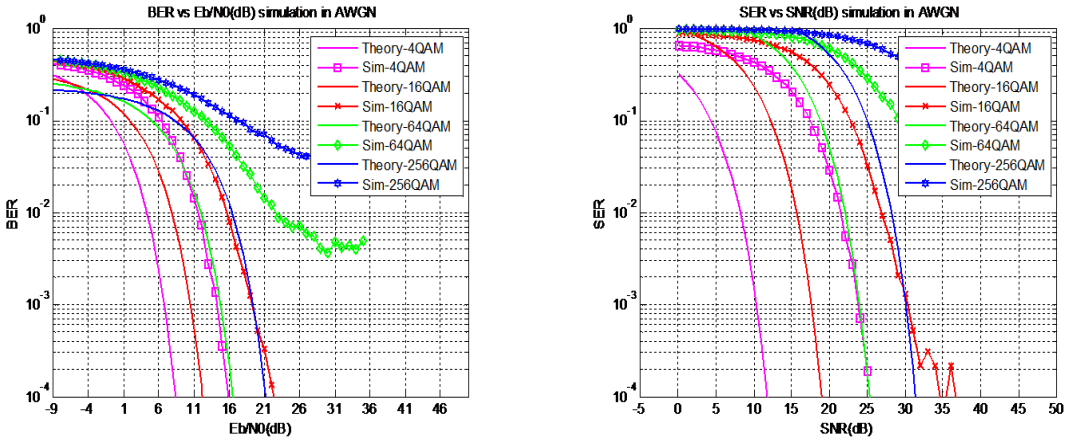

(a) BER vs E_b/N_0 (b) SER vs SNR

Figure 3.2: Simulation of conventional DCO-OFDM system.

The results shown in Figure 3.2 are consistent with the results in [5]. Due to the hard clipping after adding DC bias, the required E_b/N_0 is significantly larger than the OFDM RF system when comparing the same modulation order. Most importantly, signals modulated by 64- and 256-QAM even incur an error floor due to the clipping. Original PAPR of the DCO-OFDM system is also obtained in this simulation. According to the definition of PAPR, the threshold value, $PAPR_0$, in the simulation is determined in such a way:

Given:
Input data, Number of Input data, Step, $Max\{\text{Input data}\}$, $Min\{\text{Input data}\}$
Find:
$\chi = \text{Number of (Input data} > PAPR_0)$
$\xi(dB) = 10\log_{10}\frac{\chi}{\text{Number of Input data}}$
Constraints:
$PAPR_0 \geq Min\{\text{Input data}\}$
$PAPR_0 \leq Max\{\text{Input data}\}$
$PAPR_0 = PAPR_0 + \text{Step}$

Table 3.1: Calculation of PAPR in Monte Carlo simulation.

According to the procedure above in Table 3.1, Figure 3.3 shows the original PAPR (about 12 dB) of the DCO-OFDM system.

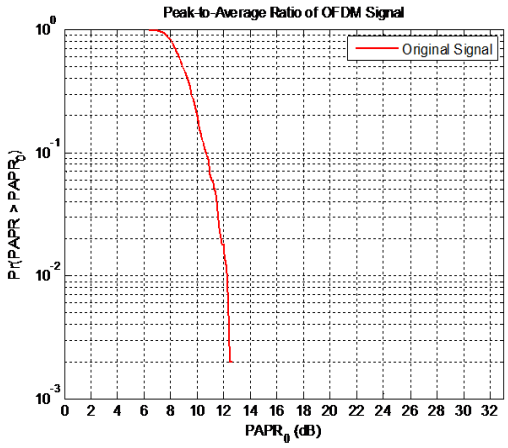

Figure 3.3: Original PAPR of conventional DCO-OFDM signal.

According to the analysis of PAPR in Chapter 2, the theoretical maximum PAPR

will reach:

$$PAPR_{max} = 10\log_{10} N = 10 \times \log_{10} 130 = 21.14dB.$$

Even though the theoretical maximum PAPR is hardly reached in most cases, it still plays an important part in evaluating the performance of the system.

3.3 ACO-OFDM system model

3.3.1 ACO-OFDM

ACO-OFDM is another commonly used technique in OWC systems based on IM/DD OFDM. In ACO-OFDM, odd subcarriers are assigned information while even subcarriers are set to zero. The data in ACO-OFDM can be constructed as:

$$\mathbf{S} = [0, S_0, 0, S_1, \ldots, 0, S_{\frac{N}{4}-1}, 0, S^*_{\frac{N}{4}-1}, 0, \ldots, S^*_1, 0, S^*_0].$$

Due to the data structure, it can be proved that the output time-domain signal, s_n, will be anti-symmetrical [37], e.g.:

$$s_k = -s_{k+\frac{N}{2}}, \qquad 0 < k < \frac{N}{2}. \tag{3.9}$$

Let $s_{m,k}$ denote the mth symbol of kth subcarrier corresponding to frequency-domain, S_m, then we have:

$$s_{m,k} = \frac{1}{\sqrt{N}} S_m e^{\frac{j2\pi km}{N}}$$

similarly,

$$\begin{aligned} s_{m,k+\frac{N}{2}} &= \frac{1}{\sqrt{N}} S_m e^{\frac{j2\pi(k+\frac{N}{2})m}{N}} \\ &= \frac{1}{N} S_m e^{\frac{j2\pi km}{N}} e^{\frac{j2\pi\frac{N}{2}m}{N}} \\ &= -\frac{1}{N} S_m e^{\frac{j2\pi km}{N}} \\ &= -s_{m,k} \end{aligned} \tag{3.10}$$

Real signals will be guaranteed by the Hermitian symmetry. To further make the signal non-negative, negative outputs will be clipped at zero. According to Eq. (3.10), negative signals can be restored by the corresponding positive signals at the receiver.

3.3.2 Analysis of clipping noise

Clipping in ACO-OFDM will generate noise power that falls on even subcarriers without affecting odd subcarriers. According to the Bussgang's theorem, the clipped signal can be expressed as:

$$s_{k,clipped} = K s_k + n_{clip} \tag{3.11}$$

where K is a constant, and n_{clip} is the clipping noise that is uncorrelated to signal s_k, e.g., $E[s_k n^*_{clip}] = 0$. Multiplying s^*_k on both sides of Eq. (3.11) and taking

expectation, then we have:

$$E[s_{k,clipped}s_k^*] = KE[s_k s_k^*] + E[n_{clip}s_k^*]$$

then the constant K can be expressed as:

$$K = \frac{E[s_{k,clipped}s_k^*]}{E[s_k s_k^*]}.$$

Since s_k is real, e.g., $s_k = s_k^*$, and symmetrically distributed about zero, as shown in Eq. (3.10), $E[s_{k,clipped}s_k] = E[s_k s_k]/2$ holds and therefore $K = 1/2$. That means the signal is reduced by half due to the clipping. It can be further shown that the received signal, $S_{k,clipped}$, is also exactly half of the transmitted signal S_k [37]. Let S_k denote the frequency-domain symbols at the receiver, that is:

$$S_k = \frac{1}{\sqrt{N}} \sum_{k=0}^{N-1} s_k e^{-\frac{j2\pi km}{N}}. \tag{3.12}$$

Considering the property of clipped signals, modify the Eq. (3.12) to derive:

$$\begin{aligned} S_k &= \frac{1}{\sqrt{N}} \sum_{\substack{k=0 \\ s_k>0}}^{\frac{N}{2}-2} \left[s_k e^{-\frac{j2\pi km}{N}} + s_{k+\frac{N}{2}} e^{-\frac{j2\pi(k+\frac{N}{2})m}{N}} \right] \\ &+ \frac{1}{\sqrt{N}} \sum_{\substack{k=0 \\ s_k<0}}^{\frac{N}{2}-2} \left[s_k e^{-\frac{j2\pi km}{N}} + s_{k+\frac{N}{2}} e^{-\frac{j2\pi(k+\frac{N}{2})m}{N}} \right] \end{aligned} \tag{3.13}$$

since odd subcarriers are non-zero and $s_k = -s_{k+\frac{N}{2}}$, the second term of Eq. (3.13) will equal to the first term in each of the superpositions, the Eq. (3.13) can be

rewritten as:

$$S_k = \frac{2}{\sqrt{N}} \sum_{\substack{k=0 \\ s_k>0}}^{\frac{N}{2}-2} s_k e^{-\frac{j2\pi km}{N}} + \frac{2}{\sqrt{N}} \sum_{\substack{k=0 \\ s_k<0}}^{\frac{N}{2}-2} s_k e^{-\frac{j2\pi km}{N}}. \tag{3.14}$$

Considering the case of clipping a signal with only odd frequencies and comparing with Eq. (3.13) by summing over the positive signal give:

$$S_{k,clipped} = \frac{1}{\sqrt{N}} \sum_{k=0}^{N-1} s_{k,clipped} e^{-\frac{j2\pi km}{N}} = \frac{S_k}{2}. \tag{3.15}$$

Clipping in this case results in the amplitude of each odd subcarrier being exactly half of the corresponding original signal and therefore the clipping noise power falls on the even subcarriers.

3.3.3 Spectral and power analysis of ACO-OFDM

Due to the data structure of ACO-OFDM, a quarter of subcarriers are used to carry information. Therefore, the achieved data rate with CP for ACO-OFDM system is given by [5]:

$$R_s^{ACO} = \left(\frac{\frac{N}{4} - 1}{N + N_{cp}} \right) B \log_2(M) = \frac{(\frac{N}{4} - 1) \log_2(M)}{(N + N_{cp})T} \quad \text{bits/s} \tag{3.16}$$

and the spectral-efficiency of the ACO-OFDM system can be expressed as:

$$\eta_{ACO} = \frac{R_s^{ACO}}{B} = \frac{(\frac{N}{4} - 1) \log_2(M)}{(N + N_{cp})} \quad \text{bits/s/Hz.} \tag{3.17}$$

For a large number of subcarriers, the amplitude of the unclipped ACO-OFDM signal, s_n, can be approximated by a Gaussian distribution. Therefore, the amplitude of the clipped signal, $s_{clipped}$, is the half-Gaussian distribution [2]:

$$f_{s_{n,clipped}}(s) = 0.5\delta(x) + \frac{u(x)}{\sigma_{s_n}\sqrt{2\pi}} e^{-\frac{s^2}{2\sigma^2_{s_n}}} \tag{3.18}$$

where $\sigma_{s_n} = E[\{s_n\}^2]$ is the standard deviation of the unclipped signal, $\delta(\cdot)$ is the Dirac delta function, and $u(\cdot)$ is the Heaviside step function. The average transmitted optical power, $P_{s(opt)}$, of the clipped signal is [8]:

$$P^{ACO}_{s(opt)} = E[s_n] = \int_{-\infty}^{\infty} s_n f_{s_{n,clipped}}(s) ds = \frac{\sigma_{s_n}}{\sqrt{2\pi}} \tag{3.19}$$

and the electrical power, $P^{ACO}_{s(elec)}$, is given by:

$$P^{ACO}_{s(elec)} = E[\{s_n\}^2] = \int_{0}^{\infty} s_n^2 f_{s_{n,clipped}}(s) ds = \frac{\sigma^2_{sn}}{2}. \tag{3.20}$$

For a fixed SNR, the BER performance is independent of the bandwidth, and consequently independent of the throughput. Therefore, the BER of the ACO-OFDM modulated by M-QAM can be calculated as:

$$BER = \frac{2(\sqrt{M}-1)}{\sqrt{M}\log_2 M} \text{erfc}\left(\sqrt{\frac{3E_s/N_0}{2(M-1)}}\right). \tag{3.21}$$

3.3.4 Simulated BER of ACO-OFDM

The BER performance of ACO-OFDM system is simulated by assuming that no channel fading and CP adding, perfect synchronization between transmitter and receiver front-ends, and noise is modulated as AWGN. The transmitted OFDM signal is normalized to unity with a given E_b/N_0 ranges from $-9dB$ to $35dB$. The number of subcarriers is set to 130, among which 32 are desirable symbols. The simulation curve is bounded by the conventional OFDM RF system, as shown in Figure 3.4.

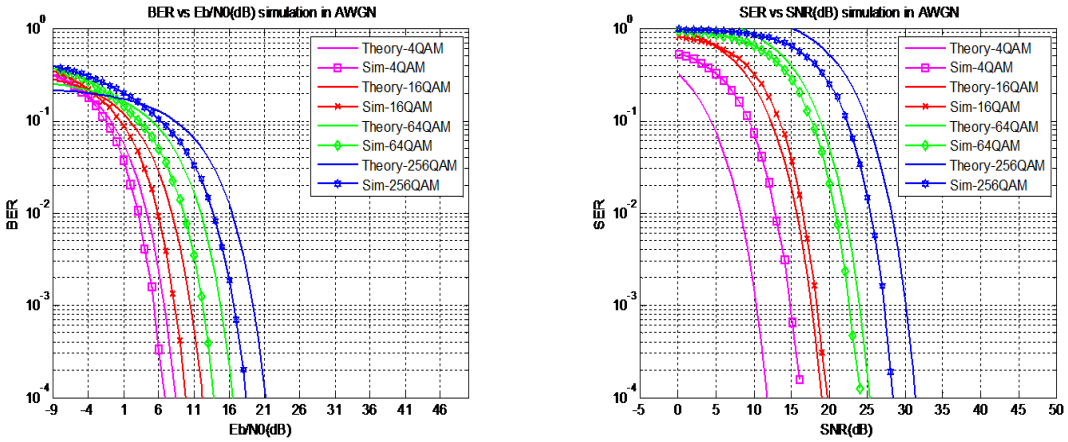

(a) BER vs E_b/N_0 (b) SER vs SNR

Figure 3.4: Simulation of conventional ACO-OFDM.

The results shown in Figure 3.4 are consistent with the results in [14]. In spite of the spectral-efficiency, ACO-OFDM system outperforms the theoretical RF OFDM system. Since ACO-OFDM signals are real and positive, received negative signals are clipped at zero, leading to the improved BER performance. The original PAPR of the ACO-OFDM (about $15dB$) is simulated, as shown in Figure 3.5.

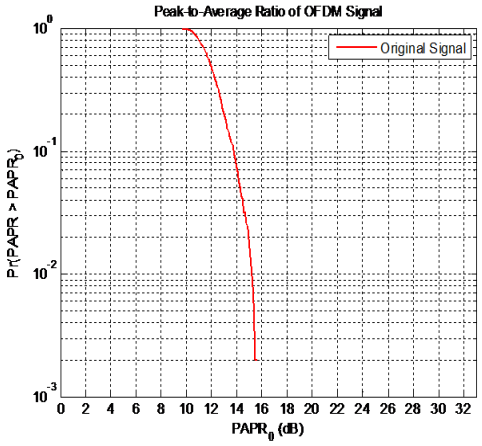

Figure 3.5: Original PAPR of ACO-OFDM system.

3.4 Modified optical OFDM systems

3.4.1 Principle of modification

To improve BER performance of optical OFDM systems, a modified model is given in this section. The principle of modification is that real OFDM samples are grouped with a zero sample to generate a new sample pair. If the original time-domain OFDM sample is positive, the first value of the new pair is set with its amplitude and the second sample of the new pair is set to zero. If the original time-domain OFDM sample is negative, the first sample of the new pair is set to zero and the second sample of the new pair is set with the corresponding positive value of the OFDM sample [34]. The model is illustrated in Figure 3.6.

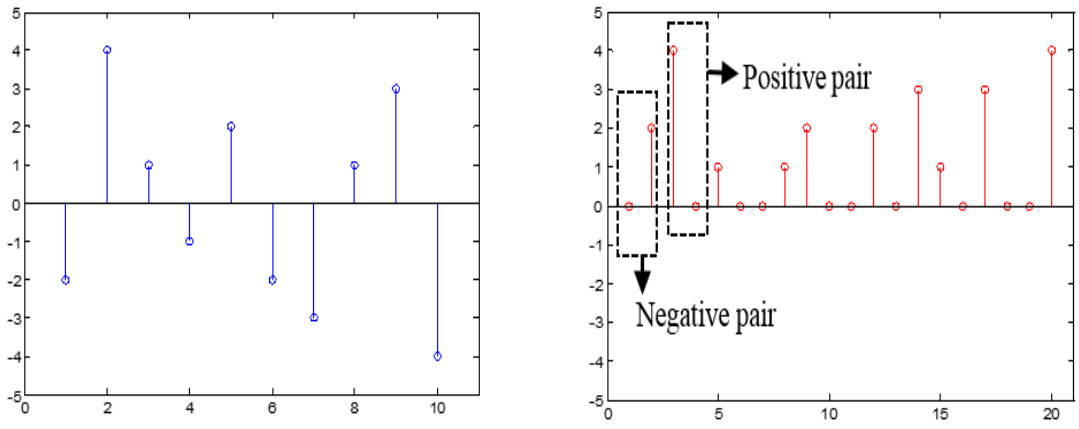

(a) Before padding zeros

(b) After padding zeros

Figure 3.6: Modified ACO-OFDM time domain signals.

By the modification, the size of OFDM frame is doubled. Since light source techniques develop rapidly, the OWC systems are able to transmit information in a higher data rate with theoretically unlimited bandwidth. Therefore, the doubled size of OFDM frame is neglected in this thesis. At the receiver, since the sign and amplitude of the original signal are denoted by each pair, signal can be recovered by comparing the amplitudes of each pair in such a way that the higher amplitude sample is considered active and the other considered passive. Let $\hat{s}_n$ denote the received time-domain signal. Then, for the DCO-OFDM system, received signal, $\hat{s}_n$, can be recovered by using:

$$\hat{s}_n = \begin{cases} \hat{s}_n, & \text{if } |\hat{s}_n| > |\hat{s}_{n+1}| \\ -\hat{s}_n, & \text{if } |\hat{s}_n| < |\hat{s}_{n+1}| \end{cases} \quad n = 0, 2, \ldots, 2N-1. \tag{3.22}$$

The received ACO-OFDM signal is given by:

$$\hat{s}_n = \begin{cases} \dfrac{\hat{s}_n - \hat{s}_{n+N/2}}{2}, & \text{if } \hat{s}_n > \hat{s}_{n+N/2} \\ \dfrac{-\hat{s}_n + \hat{s}_{n+N/2}}{2}, & \text{otherwise.} \end{cases} \tag{3.23}$$

$$\hat{s}_{n+N/2} = \begin{cases} -\dfrac{\hat{s}_n - \hat{s}_{n+N/2}}{2}, & \text{if } \hat{s}_n > \hat{s}_{n+N/2} \\ \dfrac{-\hat{s}_n + \hat{s}_{n+N/2}}{2}, & \text{otherwise.} \end{cases} \tag{3.24}$$

Since the transmitted signal is always real and positive in a IM/DD system, any negative values caused by the effect of noise can be clipped at zero, and by comparing the sample pairs, up to 50% probability of noise power will be eliminated during the inverse operation.

3.5 Summery

The OWC system is described, including the modification of data structure of RF OFDM signal. Two commonly used OWC systems, DCO-OFDM and ACO-OFDM, are analyzed and simulated. Spectral and power analysis of both systems are discussed, including their BER calculations. Clipping noise of ACO-OFDM is analyzed. A modified optical OFDM model is presented, including the detection of the received signal.

Chapter 4: Performances of M-QAM optical OFDM systems with exponential companding or zero padding

4.1 Introduction

In this chapter, DCO-OFDM and ACO-OFDM systems are simulated with either exponential companding or zero padding. Considering the spectral-efficiency of both systems, M-QAM is adopted, instead of BPSK [33] or QPSK [34]. To evaluate the performances of companding and zero padding independently, companded system is simulated, followed by zero padding system. The performances of both schemes are compared with conventional systems in terms of PAPR and required SNR. Simulations assume that there is no channel fading during transmission, perfect synchronization between the transmitter and receiver, no CP added, and with AWGN.

4.2 Performance of DCO-OFDM system

4.2.1 Companded DCO-OFDM

In this section, the companded DCO-OFDM is simulated. To generate non-negative signal, a DC bias that is twice of the average signal power is added to the transmitted signal. Figure 4.1 shows the PAPR reduction of the 256-QAM signals.

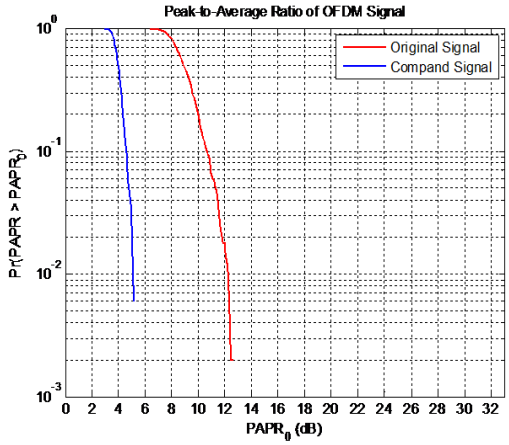

Figure 4.1: PAPR reduction of conventional DCO-OFDM system in AWGN after companding.

Through exponential companding, PAPR is reduced by about $7dB$ at a probability of $P(PAPR > PAPR_0) = 2 \times 10^{-3}$. Since exponential companding is a non-linear operation, signals suffer from distortion. BER performance of the companded system is shown in Figure 4.2. For comparison, the theoretical curves of RF OFDM systems in AWGN channels are also included. The results are shown below:

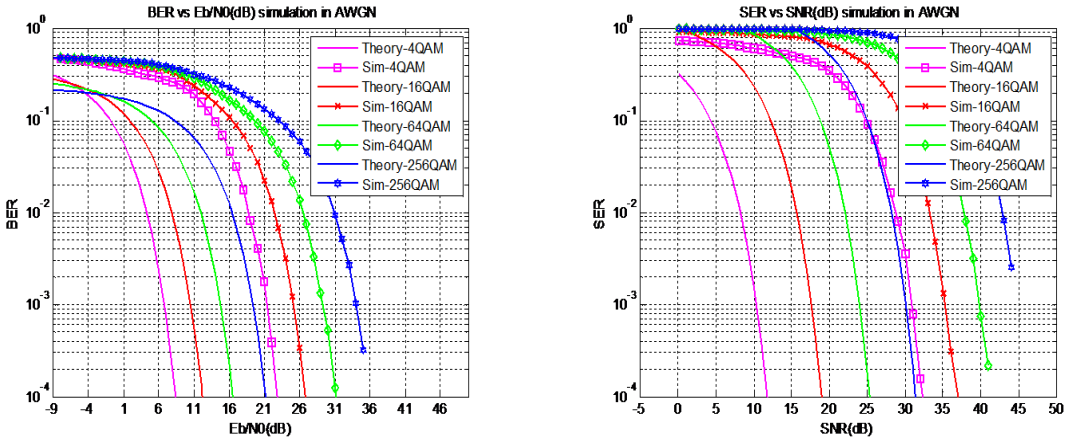

(a) BER vs E_b/N_0 (b) SER vs SNR

Figure 4.2: Simulation of conventional DCO-OFDM system with companding.

With companding, a larger E_b/N_0 is required at a target BER of 10^{-4}. However, 64-QAM and 256-QAM DCO-OFDM systems did not exhibit an error floor. The reason is that large signals are compressed while small signals are enhanced simultaneously by companding, leading to the resistance of the signal to noise.

4.2.2 Comparison of companded and conventional DCO-OFDM

In this section, we compare the performances of companded and conventional DCO-OFDM. Figure 4.3 shows the performances of both systems in terms of BER versus E_b/N_0.

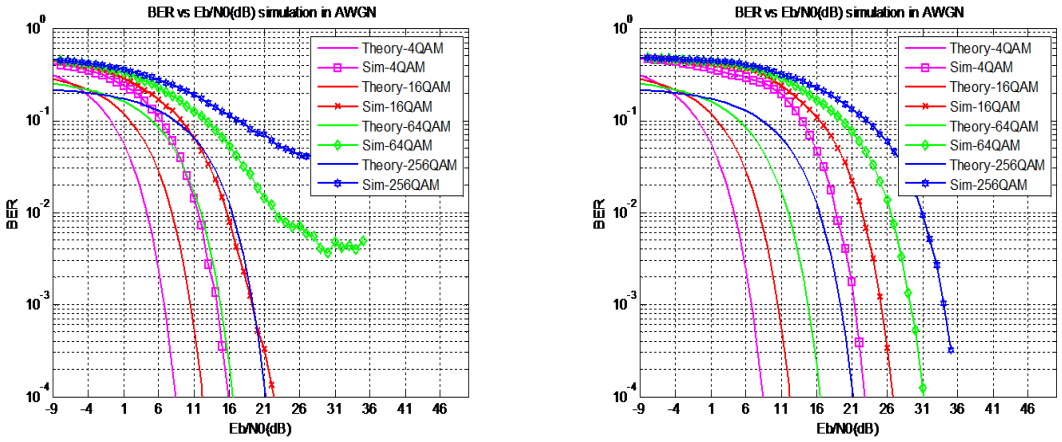

(a) Conventional DCO-OFDM (b) Companded DCO-OFDM

Figure 4.3: Comparison of conventional and companded DCO-OFDM.

It is observed that the required E_b/N_0 of the companded 4-QAM and 16-QAM systems require $6dB$ more than the conventional systems at a target BER of 10^{-4}. However, the companded 64-QAM and 256-QAM systems did not exhibit an error floor in the E_b/N_0 rang simulated.

4.2.3 Un-companded modified DCO-OFDM

The un-companded modified DCO-OFDM system with zero padding is simulated in this section. Due to zero padding, no DC bias is needed for the transmitted signal, making the system more power-efficient. Since the data in the modified system is constructed identically to the conventional DCO-OFDM before padding zeros, the modified system keeps the name DCO-OFDM for simplicity in the following sections. Figure 4.4 shows that due to the zero padding, the BER performance improves

significantly, but the spectral efficiency is reduced by a half.

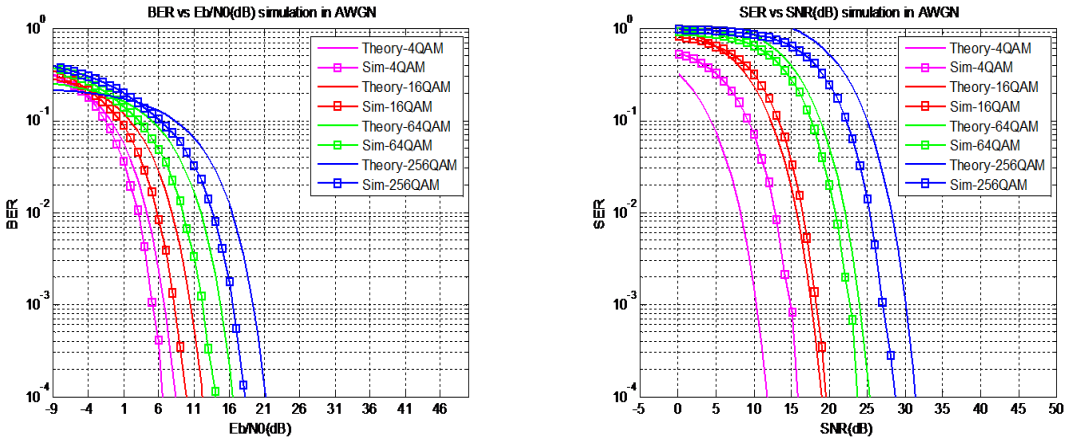

(a) BER vs E_b/N_0 (b) SER vs SNR

Figure 4.4: Un-companded modified DCO-OFDM system with zero padding in AWGN.

Figure 4.4 shows the BER performances of 64-QAM and 256-QAM with zero padding. Again, no error is exhibited in the E_b/N_0 range simulated. Considering the principle of zero padding, the average signal power is decreased by a half without changing the peak values, leading to a PAPR increase by about $3dB$, as shown in Figure 4.5.

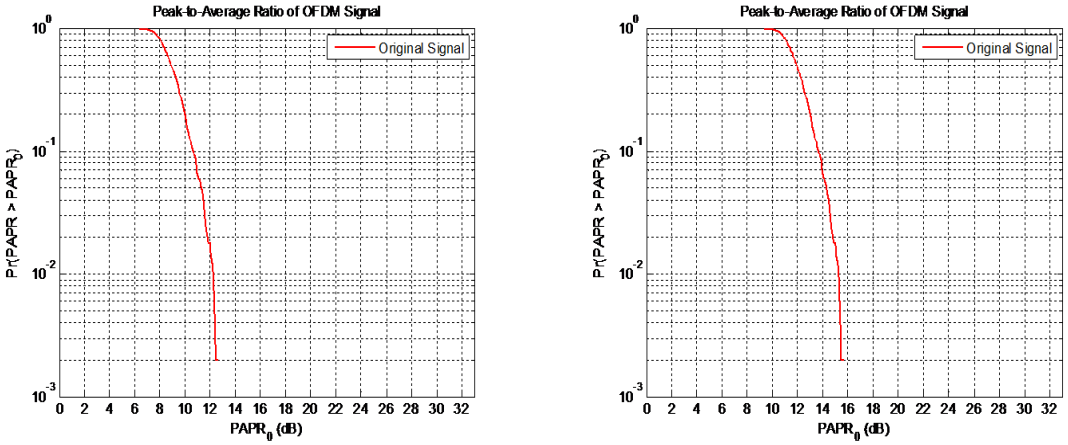

(a) PAPR of conventional DCO-OFDM

(b) PAPR of zero padding DCO-OFDM

Figure 4.5: PAPR of conventional and un-companded zero-padding-modified DCO-OFDM in AWGN.

Mathematically, that is explained as:

$$\begin{aligned} PAPR(dB)_{Modified} = \frac{P_{peak}}{P_{average}} &= 10log_{10}\frac{\max\limits_{0<n<N-1}[|s_n|^2]}{E[|s_n|^2]/2} \\ &= 10log_{10}2 + PAPR_{Conventional} \\ &= 3(dB) + PAPR_{Conventional}. \end{aligned}$$

The performances of the conventional DCO-OFDM and the un-companded zero-padding-modified DCO-OFDM are compared in Figure 4.6, where the conventional DCO-OFDM is denoted by square-solid curves, and the un-companded zero-padded modified system is presented by star-solid curves.

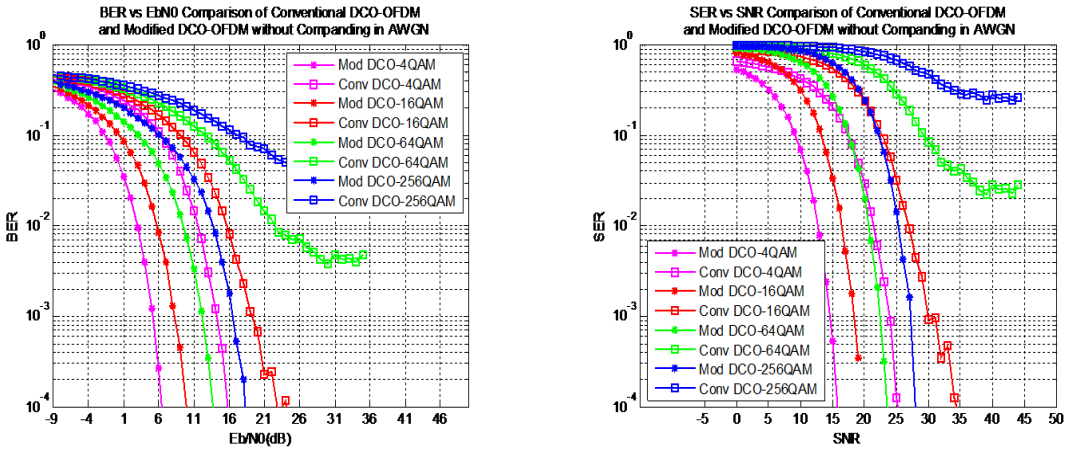

(a) BER vs E_b/N_0 (b) SER vs SNR

Figure 4.6: Comparison of conventional and un-companded zero-padding-modified DCO-OFDM in AWGN.

The un-companded zero-padded modified DCO-OFDM significantly outperforms the conventional system. For example, the zero padding modified 4-QAM system requires about $6dB$ E_b/N_0 at a target BER of 10^{-4}, while the conventional 4-QAM system requires $16dB$ to reach the same target BER. As the modulation order increases, the improvement is more significant. More importantly, the zero padding modified DCO-OFDM is not DC biased and therefore is more power-efficient without introducing clipping noise to the signals.

4.3 Performance of ACO-OFDM systems

4.3.1 Companded ACO-OFDM

In this section, the companded ACO-OFDM system with M-QAM is simulated. As the DCO-OFDM case, we assume that there is no channel fading during transmis-

sion, ideal synchronization between the transmitter and receiver, no CP added, and noise is modulated as AWGN. Figure 4.7 shows the PAPR reduction of the system.

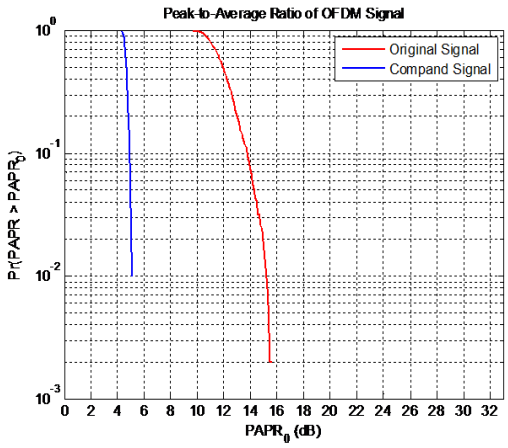

Figure 4.7: PAPR reduction of conventional ACO-OFDM.

By using exponential companding, PAPR is reduced by approximately $10dB$. However, the system is significantly distorted by the non-linear operation of companding. BER performance of the companded ACO-OFDM is shown in Figure 4.8, where the theoretical BER curves of conventional RF OFDM systems in AWGN are also included.

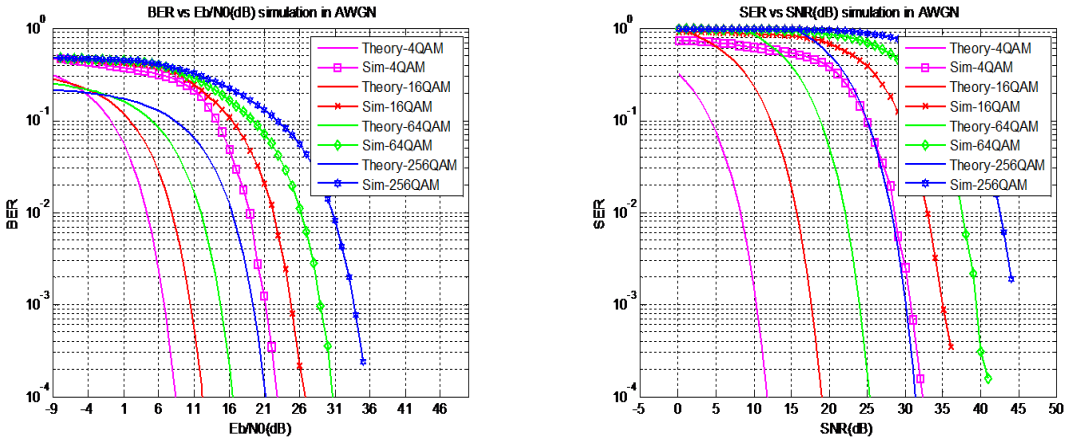

(a) BER vs E_b/N_0 (b) SER vs SNR

Figure 4.8: Simulation of companded ACO-OFDM in AWGN.

Figure 4.8 is based on the assumption that the same PAPR reduction is achieved in both companded DCO-OFDM and ACO-OFDM systems. Due to the data property of ACO-OFDM system discussed in Chapter 3, signals are distorted more significantly than the companded DCO-OFDM.

4.3.2 Comparison of companded and conventional ACO-OFDM

In this section, we compare the performances of campanded and conventional ACO-OFDM. Figure 4.9 shows the performances of both systems in terms of BER versus E_b/N_0.

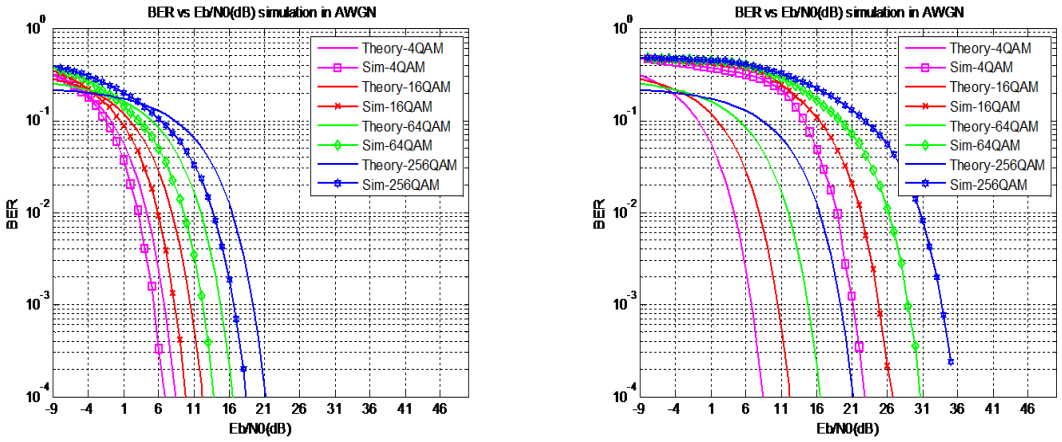

(a) Un-companded ACO-OFDM (b) Companed ACO-OFDM

Figure 4.9: Comparison of companded and un-companed ACO-OFDM in AWGN.

Note that the PAPR of the companded ACO-OFDM is reduced by about $7dB$. The required E_b/N_0 of the companded system is largely increased. For example, in the case of 4-QAM, the companded ACO-OFDM requires about $23dB$ E_b/N_0 at the target BER of 10^{-4}, compared with approximate $7dB$ in the conventional system. Furthermore, as the modulation order increases, the increment of E_b/N_0 is getting larger.

4.3.3 Un-companded zero-padding-modified ACO-OFDM

The un-companded ACO-OFDM system with zero padding is simulated in this section. Due to the reservation of negative signals, the spectral-efficiency of the zero-padding-modified ACO-OFDM remains the same as the conventional system. The BER performance is shown in Figure 4.10.

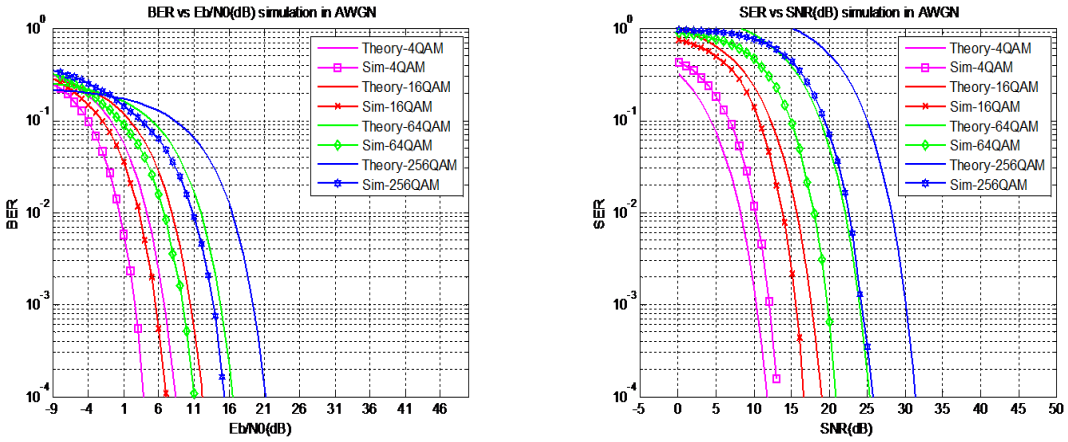

(a) BER vs E_b/N_0 (b) SER vs SNR

Figure 4.10: Simulation of modified ACO-OFDM without companding in AWGN.

From Figure 4.10, it can be seen that the zero-padding-modified ACO-OFDM without companding has an outstanding BER performance. Without clipping the negative signals and changing the average signal power, the PAPR in the modified ACO-OFDM remains the same as the conventional system, as shown in Figure 4.11.

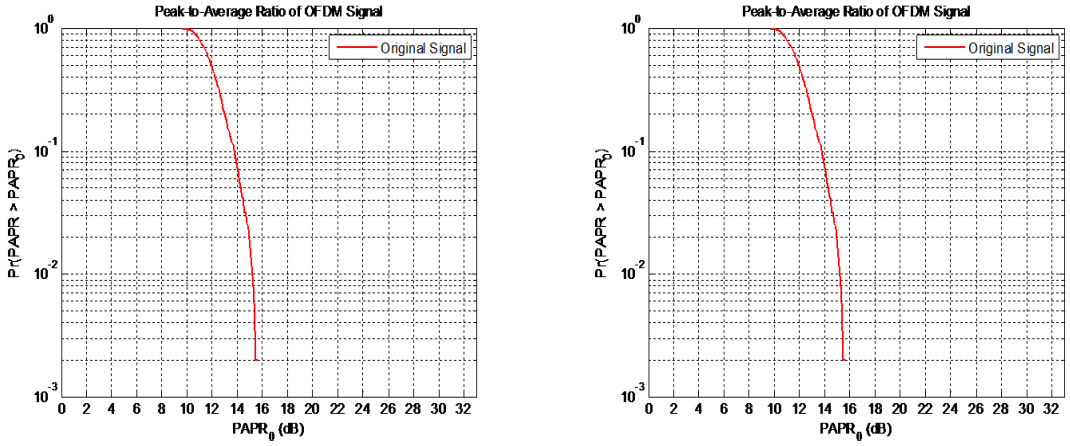

(a) PAPR of the modified system

(b) PAPR of the conventional system

Figure 4.11: Original PAPR of the zero-padding-modified and conventional ACO-OFDM systems.

The performances of the conventional ACO-OFDM and the un-companded zero-padding-modified ACO-OFDM is compared in Figure 4.12, where the conventional ACO-OFDM is denoted by square-solid curves, and the zero-padding-modified ACO-OFDM is denoted by stat-solid curves. Considering the identical spectral-efficiency of both systems, simulations modulated by the same order are compared.

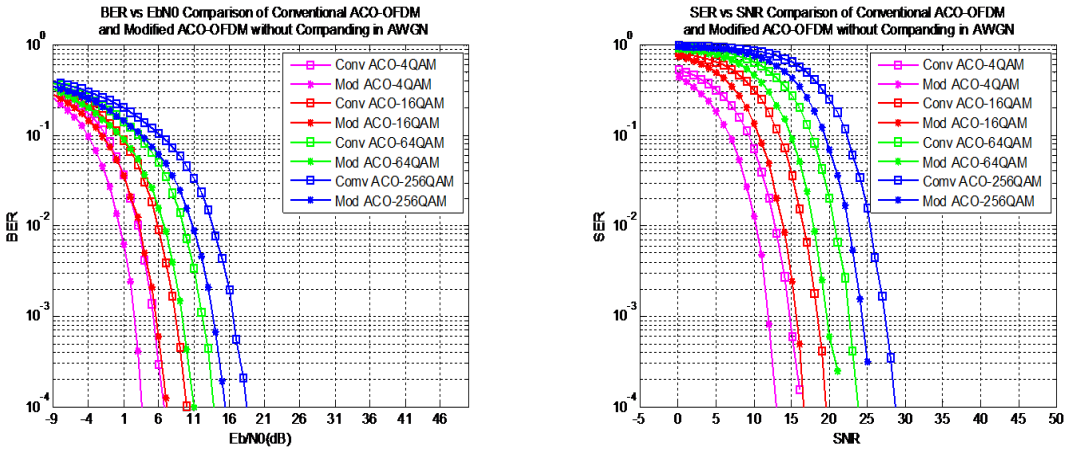

(a) BER vs E_b/N_0 (b) SER vs SNR

Figure 4.12: Comparison of the conventional and un-companded zero-padding-modified ACO-OFDM in AWGN.

In the case of 4-QAM, it is observed from Figure 4.12 a) that the performance of the modified ACO-OFDM compared with conventional system is better by approximate $3dB$. That is due to the zero padding, 50% probability of noise power is clipped at the receiver when detecting active signals.

4.4 Summery

In this chapter, the M-QAM DCO-OFDM and ACO-OFDM systems are simulated with either exponential companding or zero padding. Exponential companding shows an outstanding capability in reducing PAPR. The BER performances of the 64-QAM and 256-QAM DCO-OFDM systems are improved by companding. The companded ACO-OFDM system suffers from more distortion due to the fact that the signal is halved to generate a real value. Considering the large required SNR

caused by the non-linear operation of companding, zero-padding-modified DCO-OFDM and ACO-OFDM are introduced and simulated. Due to the modification, the BER performances of both systems are significantly improved at an expense of spectral-efficiency.

Chapter 5: Optimization of Optical OFDM Systems

5.1 Optimized DCO-OFDM system

Considering the capabilities of exponential companding and zero padding in reducing the PAPR and the required SNR, respectively, the DCO-OFDM system is optimized by combining both schemes in this section. Due to zero padding, no DC bias is needed for the transmitted signal, making the system more power-efficient. Since the data in the optimized system is constructed identically to the conventional DCO-OFDM before padding zeros, the optimized system is still called DCO-OFDM for simplicity in the following sections. Simulation is shown in Figure 5.1, where the theoretical BER curves of RF OFDM systems in AWGN are included. Figure 5.2 shows the PAPR reduction of the optimized system.

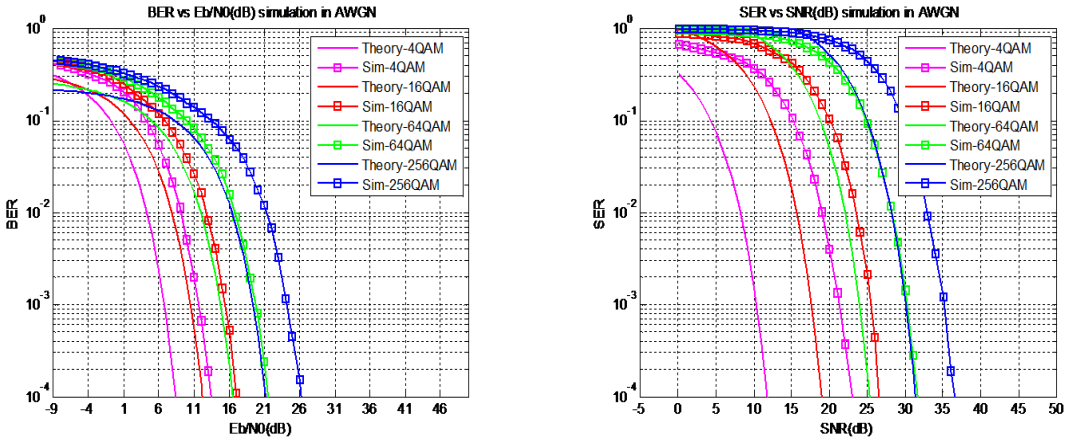

(a) BER vs E_b/N_0 (b) SER vs SNR

Figure 5.1: Simulation of optimized DCO-OFDM.

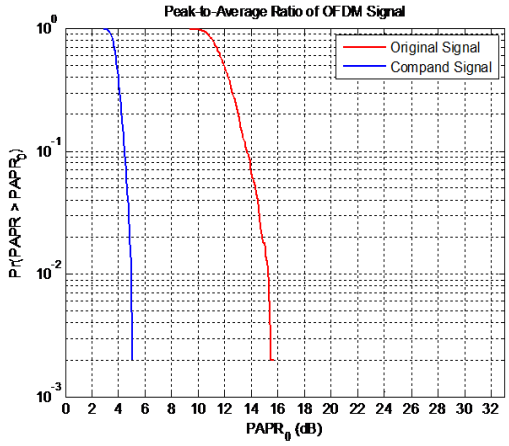

Figure 5.2: PAPR reduction of optimized DCO-OFDM.

By the combination, the DCO-OFDM is improved significantly with slightly increasing the required E_b/N_0. In the case of 256-QAM as shown in Figure 5.1 a), the optimized DCO-OFDM requires $26dB$ E_b/N_0 to reach the target BER of 10^{-4} with about $10dB$ PAPR reduction shown in Figure 5.2. Furthermore, systems modulated

by higher orders show a better improvement. The reason is that the clipped noise power plays a more important part in the higher-order modulation systems when detecting and demodulating the received signals.

5.1.1 Comparison of companded and optimized DCO-OFDM

In the condition of achieving the same PAPR reduction, the companded DCO-OFDM is compared with the optimized system in term of BER. Both systems have the same initial setups, including the number of transmitted symbols, companding degree, no CP added, unity transmitting signal power, and AWGN channel. The comparison is shown in Figure 5.2, in which star-solid curves denote the optimized system, and square-slide curves present the companded system.

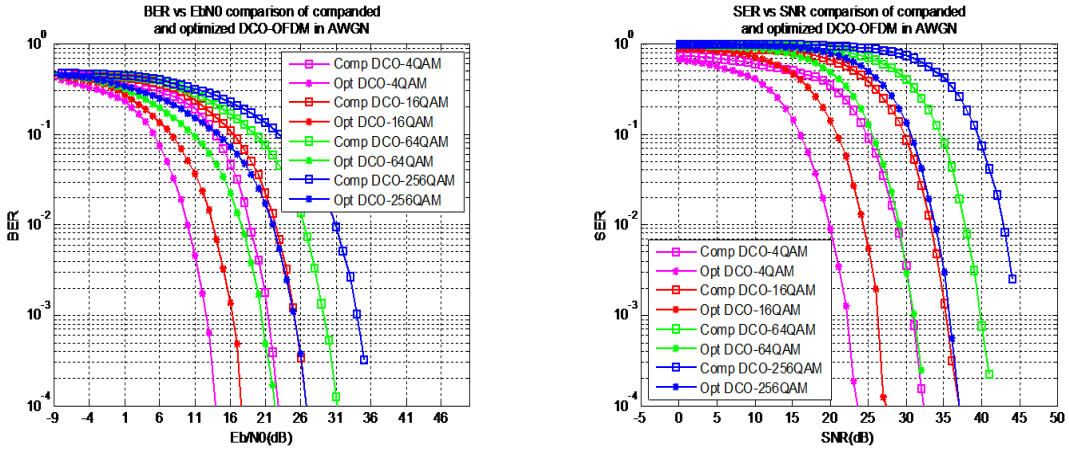

(a) BER vs E_b/N_0 (b) SER vs SNR

Figure 5.3: Comparison of optimized DCO-OFDM and companded DCO-OFDM.

The optimized DCO-OFDM requires less transmitted power than the companded

system when reducing the same PAPR. Figure 5.3 a) shows that in the case of 4-QAM, the optimized system is $8dB$ better than the companded system, and is getting better when the modulation order increases. For example, the 256-QAM optimized system is approximate $10dB$ better than the 256-QAM companded system. Note that the companded DCO-OFDM has a DC bias of twice the transmitting signal power. Generally, a DC bias will also weaken the information-carried alternative current (AC) signal, resulting in a complicated computation and circuit at the receiver.

5.1.2 Comparison of optimized and un-companded zero-padding-modified DCO-OFDM

There is always a trade-off between PAPR and SNR, that is,

$$PAPR \propto \frac{1}{E[|s|^2]}$$
$$SNR \propto E[|s|^2]$$

in this section, a slightly increased SNR caused by companding is observed in the optimized DCO-OFDM with an approximate $10dB$ PAPR reduction, compared with the un-companded zero-padding-modified system. The comparison is shown in Figure 5.4.

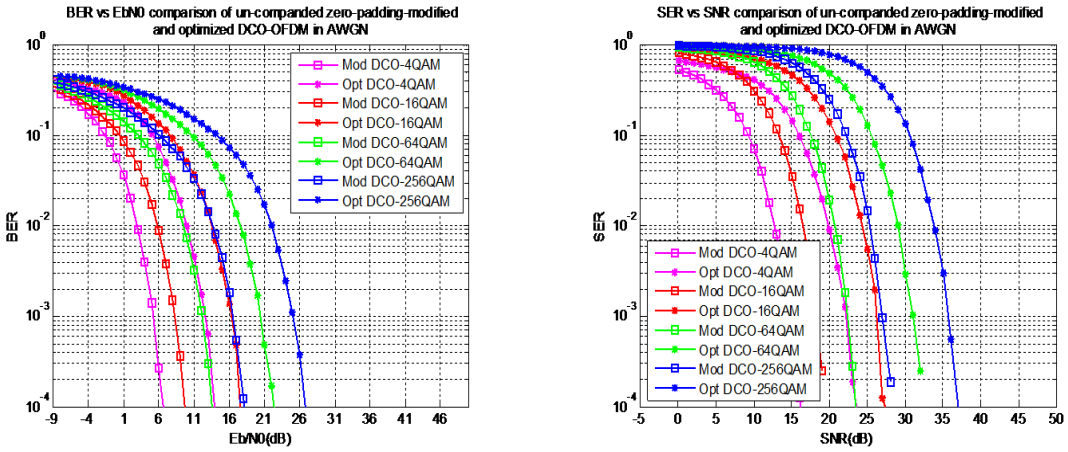

(a) BER vs E_b/N_0 (b) SER vs SNR

Figure 5.4: Comparison of the optimized and un-companded zero-padding-modified DCO-OFDM.

It can be seen from Figure 5.4 a) that the 256-QAM optimized DCO-OFDM system requires about $26dB$ E_b/N_0 at the target BER of 10^{-4}, compared with about $18dB$ of the un-companded zero-padding-modified system. A more practical way to determine the proper PAPR and the required SNR is to analyze the overall system based on the circuit components.

5.2 Optimized ACO-OFDM system

In this section, the optimized ACO-OFDM system is simulated by combining the exponential companding and zero padding. The PAPR of the optimized system is obtained as shown in Figure 5.5.

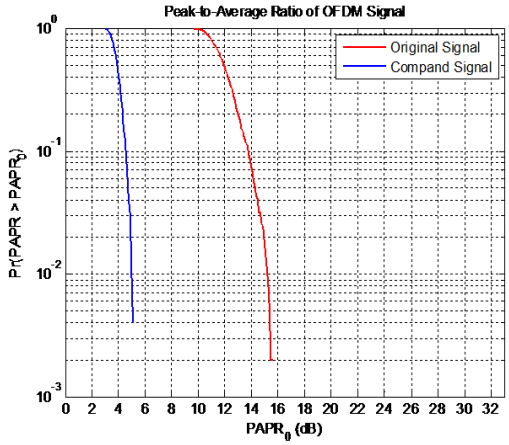

Figure 5.5: PAPR reduction of modified ACO-OFDM.

The PAPR is reduced by approximate $10dB$ in the optimized ACO-OFDM. Considering the non-linear effect of companding process, the BER performance of the optimized system is simulated, from which it can be seen that the distortion is efficiently relieved by zero padding. Due to the reservation of negative signals, the average signal power and spectral-efficiency of the optimized system remain unchanged. The simulation is shown in Figure 5.6, where the theoretical BER curves of conventional RF OFDM system in AWGN is also included.

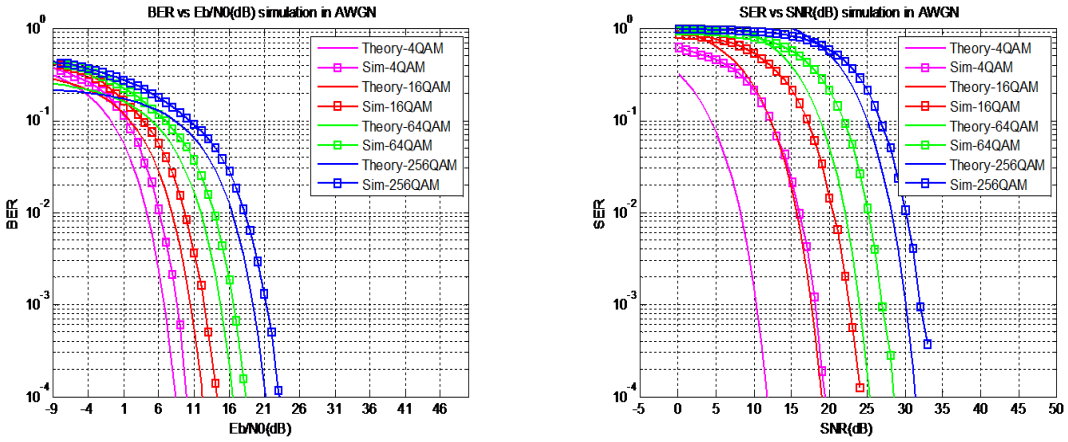

(a) BER vs E_b/N_0 (b) SER vs SNR

Figure 5.6: Simulation of optimized ACO-OFDM.

Due to the combination, the ACO-OFDM system is optimized with a slightly increased E_b/N_0. For example, in the case of 256-QAM, the optimized ACO-OFDM requires about $23dB$ E_b/N_0 at the target BER of 10^{-4}.

5.2.1 Comparison of optimized and companded ACO-OFDM

By comparing the optimized and companded ACO-OFDM systems, it can be seen that the companded ACO-OFDM system is significantly improved by the combination as shown in Figure 5.7, in which the star-solid curves denote the optimized ACO-OFDM and the square-solid curves present the companded system.

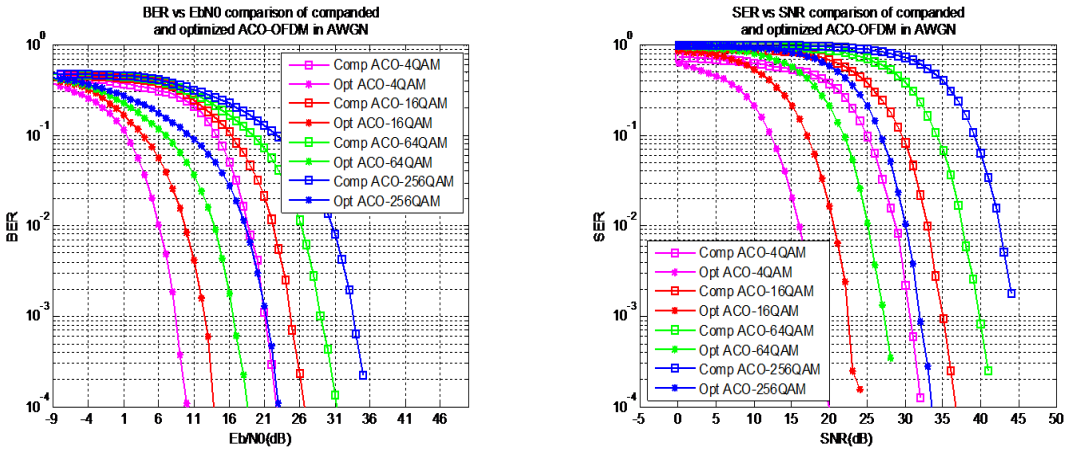

(a) BER vs E_b/N_0 (b) SER vs SNR

Figure 5.7: Comparion of optimized ACO-OFDM and companded ACO-OFDM.

Considering the case of 4-QAM, the E_b/N_0 of the optimized ACO-OFDM system is reduced approximate $12dB$ with the same PAPR reduction as the companded system. The simulation also shows that the required E_b/N_0 is reduced more efficiently as the modulation order increases.

5.2.2 Comparison of optimized and zero-padding-modified ACO-OFDM

By comparing the optimized ACO-OFDM system with the zero-padding-modified system in this section, it can be seen that the BER performance of the optimized system is degraded slightly by the companding as Figure 5.8 shows, where the optimized system is denoted by star-solid curves, and the zero-padding-modified system is denoted by square-solid curves.

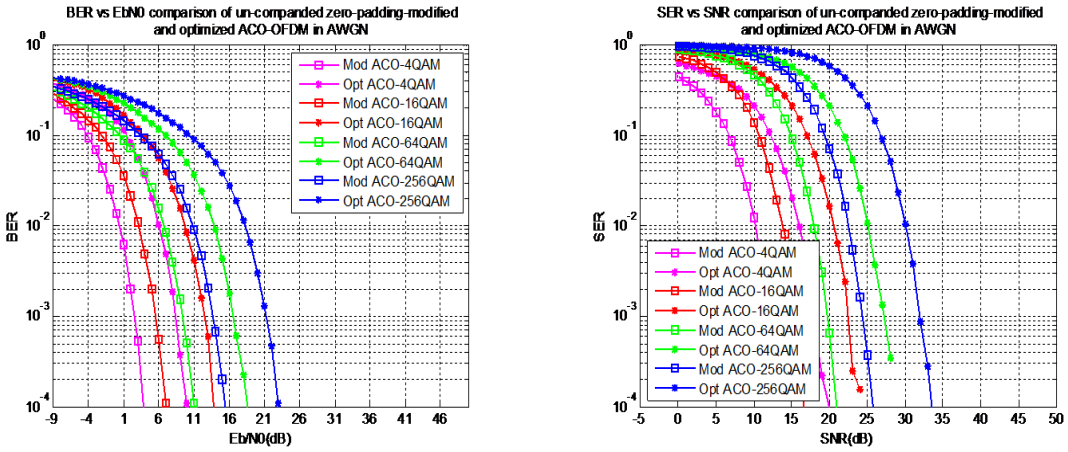

(a) BER vs E_b/N_0 (b) SER vs SNR

Figure 5.8: Comparison of optimized and un-companded zero-padding-modified ACO-OFDM.

Due to the non-linear effect of the companding process, the optimized system with approximate $10dB$ PAPR reduction has about $7dB$ increment of the required E_b/N_0 in the case of 256-QAM, compared with the zero-padding-modified system.

5.3 Comparison of optimized DCO-OFDM and ACO-OFDM

The BER performance of the optimized DCO-OFDM and ACO-OFDM is compared in this section in the condition of the same PAPR reduction. The comparison is shown in Figure 5.9, in which the optimized DCO-OFDM system is presented by star-solid curves, and the optimized ACO-OFDM system is presented by square-solid curves.

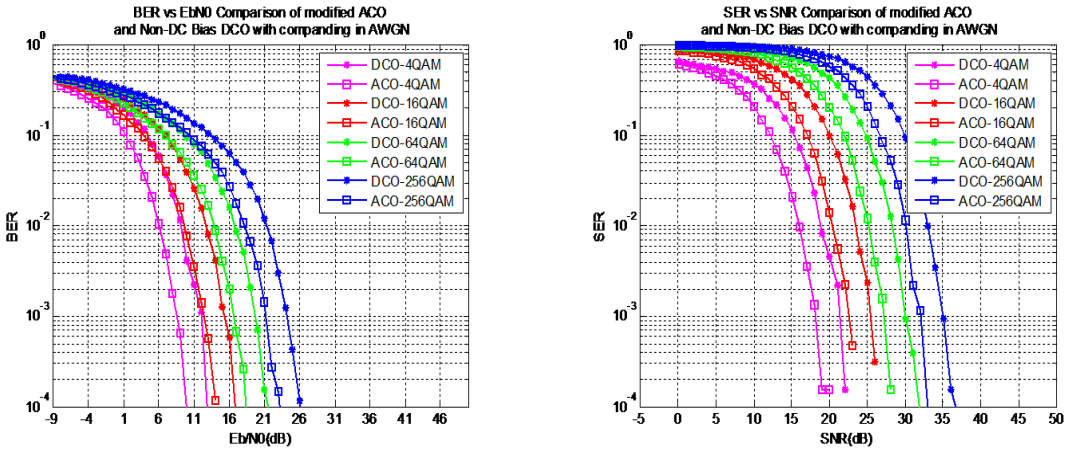

(a) BER vs E_b/N_0 (b) SER vs SNR

Figure 5.9: Comparison of optimized DCO-OFDM and ACO-OFDM.

It can be seen that the optimized ACO-OFDM system outperforms the optimized DCO-OFDM system when the same modulation order is compared. For example, in the case of 256-QAM, the optimized ACO-OFDM system is better than the optimized DCO-OFDM by $3dB$. When considering to achieve a similar spectral-efficiency, the 256-QAM ACO-OFDM system should be compared with the 64-QAM DCO-OFDM. In this case, the optimized DCO-OFDM system outperforms the optimized ACO-OFDM by about $2dB$. This is due to the fact that more noise power is clipped in the optimized DCO-OFDM system when inversely operating the zero padding process, and DCO-OFDM system is able to deliver more information when the same OFDM signal frame is constructed.

5.4 Summery

In this chapter, the optimized DCO-OFDM and ACO-OFDM systems are implemented by combining the exponential companding and zero padding techniques. The PAPR of the optimized systems are significantly reduced at the expense of slightly increasing the required SNR. Both systems are compared with their companded or zero padding systems. At the end the the chapter, comparison of the optimized DCO-OFDM and ACO-OFDM is given when the same PAPR is reduced.

Chapter 6: Conclusion

6.1 Main implementations

This thesis presented a scheme that combines exponential companding with zero padding to reduce the PAPR and required SNR of DCO-OFDM and ACO-OFDM systems. The PAPR is reduced about $10dB$ in the proposed systems with significantly improved BER performance. The proposed DCO-OFDM and ACO-OFDM systems require $26dB$ and $23dB$ bit-to-noise ratio, respectively, at the target BER of 10^{-4} when signals are modulated by 256-QAM. Through combination, the DCO-OFDM system is optimized that no DC bias is added to the transmitted signals, and the ACO-OFDM system is improved in terms of PAPR reduction without being increased the spectral-efficiency by zero padding.

The motivation of the thesis is presented, followed by the backgrounds of OWC and OFDM systems. In order to employ OFDM to the OWC systems, modifications of the data structure is given by imposing the Hermitian symmetry. Two commonly used OWC systems, DCO-OFDM and ACO-OFDM, are analyzed and simulated. The drawback of OFDM systems, PAPR, is discussed, including its solution called exponential companding. Considering the distortion of companding, another solution for the required SNR called zero padding is also given. In this thesis, companded or zero padding systems are simulated and compared with the conventional systems. By combining both schemes, the optimized systems are proposed with their parison

of either companded or zero padding systems.

6.2 Limitations of work, outlook, and future work

The analytical models of OFDM-based OWC systems have been shown to be in very close agreement with an equivalent Monte Carlo simulation. However, there are a couple of essential assumptions which have been made for the sake of straightforward derivations. The following suggestions can be considered to improve the performance of the OWC system in practical single-link and multi-user implementation setups.

First, the models of DCO-OFDM and ACO-OFDM systems rely on the assumption that the time-domain OFDM signal follows close to Gaussian distribution. This is implemented based on the pre-condition that a total number of sub-carriers is greater than 64. However, when the computational resources of the electronics in the system implementation are limited, only a smaller number of IFFT/FFT operations can be processed with reasonable data rates. Therefore, a mathematical expression of IFFT/FFT, whose size is below 64, is still to be derived for a closer form of practical system. Furthermore, in this thesis, synchronization between transmitter and receiver is assumed to be ideal in that no time delay happens to both front-ends, and pulse shaping and matched filtering are assumed to be optimal in that no extra noise power or information loss is introduced. Moreover, channel knowledge at the receiver and the transmitter is assumed to be obtained, and the quantization noise in the digital-to-analog (D/A) and analog-to-digital (A/D) conversions is neglected.

So, a study of the effect of these system blocks on the front-ends can be considered in future work.

In addition, the system models and the optimum front-end setups are currently considered in a single-link OWC scenario. To improve the capacity of the system, multiple LEDs used at the transmitter, and multiple photodiodes (PDs) at the receiver are still an open issue. Future work can include the study of the OWC system that is expanded with the simulation and optimization of multiple access scenarios in a network of mobile users. Current OWC systems with IM/DD can hardly utilize the entire available optical spectrum. In addition, wavelength reuse of cellular OWC systems can be implemented without decreasing the capacity, due to the fact that center wavelength is much larger than the modulation bandwidth of the optical front-ends. An optimal organization of LEDs in multi-access network can achieve a better power efficiency and BER performance. Therefore, future work can focus on the study of the optimization of organization of transmitters and wavelength reuse for a better throughput and power consumption.

Bibliography

[1] G. Research and T. Rep., "Visible light communication (vlc)- a potential solution to the global wireless spectrum shortage," 2011, [Online].Available: http://www.gbiresearch.com.

[2] Dimitrov and S. Dimitrov, "Analysis of ofdm-based intensity modulation techniques for optical wireless communications," 2013, [Online].Available: http://hdl.handle.net/1842/7833.

[3] Y.Tanaka, T.Komine, S.Haruyama, and M.Nakagawa, "Indoor visible communication utilizing plural white leds as lighting," in *Proc. of the 12th IEEE International Symposium on Personal, Indoor and Mobile Radio Communications*, vol. 2, Sep.30-Oct.3 2001, pp. 81–85.

[4] J.Kahn and J.Barry, "Wireless infrared communications," *Proc.IEEE*, vol. 85, no. 2, pp. 265–298, Feb. 1997.

[5] Z. Ghassemlooy, W. Popoola, and S. Rajbhandari, *"Optical wireless communications: system and channel modelling with Matlab®"*. CRC Press, 2012.

[6] F.R.Gfeller and U.Bapst, "Wireless in-house data communication via diffuse infrared radiation," vol. 67, no. 11, Nov. 1979, pp. 1474–1486.

[7] H.Elgala, R.Mesleh, H.Haas, and B.Pricope, "Ofdm visible light wireless communication based on white leds," in *Proc.of the 64th IEEE Vehicular Technology Conference (VTC)*, Apr.22-25, 2007.

[8] H.Elgala, R.Mesleh, and H.Haas, "Non-linearity effects and predistortion in optical ofdm wireless transmission using leds," *International Journal of Ultra Wideband Communications and Systems*, vol. 1, no. 2, pp. 143–150, 2009.

[9] H. Elgala, R.Mesleh, and H.Haas, "Predistortion in optical wireless transmission using ofdm," in *Proc. of the 9th International Conf. on Hybrid Intelligent Systems(HIS)*, vol. 2, Aug. 2009, pp. 184–189.

[10] H.Elgala, R.Mesleh, and H.Haas, "Indoor optical wireless communication: potential and state-of-the-art," *Communications Magazine,IEEE*, vol. 49, no. 9, pp. 56–62, 2011.

[11] Mossaad and Mohammed, "Theoretical analysis and simulation of im/dd optical ofdm systems," 2011, [Online].Available:http://publishresearch.com.

[12] M. Z. Afgani, H. Haas, H. Elgala, and D. Knipp, "Visible light communication using ofdm," in *Proc. of the 2nd International Conference on Testbeds and Research Infrastructures for the Development of Networks and Communities (TRIDENTCOM)*, Mar.1-3, 2006, pp. 129–134.

[13] Y. Wu and W. Zou, "Orthogonal frequency division multiplexing: a multi-carrier modulation scheme," *IEEE Trans. Consumer Electronics.*, vol. 41,Issue 3, pp. 392–399, 1995.

[14] J.Armstrong and B.Schmidt, "Comparison of asymmetrically clipped optical ofdm and dc-biased optical ofdm in awgn," *Communications Letters,IEEE*, vol. 12, no. 5, 2008.

[15] J.Armstrong, "Ofdm for optical communications," *Journal of Lightwave Technology*, vol. 27, no. 3, pp. 189–204, Feb. 2009.

[16] J.Armstrong, B.Schmidt, D.Kalra, H.A.Suraweera, and A.J.Lowery, "Performance of asymmetrically clipped optical ofdm in awgn for an intensity modulated direct detection system," in *Proc. of IEEE Conf. on Global Telecommunications*, Nov. 2006, pp. 1–5.

[17] S.K.Wilson and J.Armstrong, "Digital modulation techniques for optical asymmetrically-clipped ofdm," in *Proc. of IEEE Conf. on Wireless Communications and Networking*, Mar. 2008, pp. 538–542.

[18] S. H. Han and J. H. Lee, "An overview of peak-to-average power ratio reduction techniques for multicarrier transmission," *IEEE Personal Communications*, vol. 12, no. 2, pp. 56–65, Apr. 2005.

[19] R.J.Baxley and G.T.Zhou, "Comparing selected mapping and partial transmit sequence for par reduction," *IEEE Trans. Broadcasting*, vol. 53, Issue 4, pp. 797–803, Dec. 2007.

[20] S.J.Heo, H.S.Noh, J.S.No, and D.J.Shin, "A modified slm scheme with low complexity for papr reduction of ofdm systems," *IEEE Trans.Broadcasting*, vol. 53, no. 4, pp. 804–808, Dec. 2007.

[21] R.W.Bauml, R.F.H.Fischer, and J.B.Huber, "Reducing the peak-to-average power ratio of multicarrier modulation by selected mapping," *IEEE Electron. Lett.*, vol. 32, no. 22, pp. 2056–2057, Oct. 1996.

[22] I. Baig and V.Jeoti, "Dct precoded slm technique for papr reduction in ofdm systems," in *Proc. of International Conf. on Intelligent and Advanced Systems (ICIAS)*, June 2010, pp. 1–6.

[23] D.-W. Lim, J.-S. No, C.-W. Lim, and H. Chung, "A new slm ofdm scheme with low complexity for papr reduction," *IEEE Signal Processing Lett.*, vol. 12, no. 2, pp. 93–96, Feb. 2005.

[24] C.-L. Wang and Y. Ouyang, "Low-complexity selected mapping schemes for peak-to-average power ratio reduction in ofdm systems," *IEEE Trans. Signal Processing*, vol. 53, no. 12, pp. 4652–4660, Dec. 2005.

[25] T. Jiang, W. Xiang, P. Richardson, J. Guo, and G. Zhu, "Papr reduction of ofdm signals using partial transmit sequences with low computational complexity," *IEEE Trans. Broadcasting*, vol. 53, no. 3, pp. 719–724, Sep. 2007.

[26] A.D.S.Jayalath and C.Tellambura, "Adaptive pts approach for reduction of peak-to-average power ratio of ofdm signal," *Electron. Lett.*, vol. 36,Issue 4, pp. 1226–1228, July 2000.

[27] W. S. Ho, A.S.Madhukumar, and F.Chin, "Peak-to-average power reduction using partial transmit sequences: a suboptimal approach based on dual layered phase sequencing," *IEEE Trans. Broadcasting*, vol. 49, no. 2, pp. 225–231, June 2003.

[28] W. .Aziz, E.Ahmed, G.Abbas, S.Saleem, and Q.Islam, "Papr reduction in ofdm using clipping and filtering," *World Applied Sciences Journal*, vol. 18, no. 11, pp. 1495–1500, 2012.

[29] X. Li and L.J.Cimini, "Effects of clipping and filtering on the performance of ofdm," in *Proc. of the 47th IEEE Conf. on Vehicular Technology Conference*, vol. 3, May 1997, pp. 1634–1638.

[30] X. Wang, T.T.Tjhung, and C.S.Ng, "Reduction of peak-to-average power ratio of ofdm system using a companding technique," *IEEE Trans. Broadcasting*, vol. 45, no. 3, pp. 303–307, Sep. 1999.

[31] T. Jiang, Y. Yang, and Y.-H. Song, "Companding technique for papr reduction in ofdm systems based on an exponential function," in *Proc. of IEEE Conf. on Global Telecommunications*, vol. 5, Dec. 2005, p. 4.

[32] J. Tao, Y. Yang, and S. Y. Hua, "Exponential companding technique for papr reduction in ofdm systems," *IEEE Trans.Broadcasting*, vol. 51, no. 2, pp. 244–248, 2005.

[33] K.Bandara, P.Niroopan, and Y.-H. Chung, "Papr reduced ofdm visible light communication using exponential nonlinear companding," in *Proc. of IEEE International Conf. on Microwaves, Communications, Antennas and Electronics Systems (COMCAS)*, Oct. 2013, pp. 1–5.

[34] S.D.Mohamed, H.S.Khallaf, H.Shalaby, I.Andonovic, and M.H.Aly, "Two approaches for the modified asymmetrically clipped optical orthogonal frequency division multiplexing system," in *Proc. of the Japan-Egypt International Conf. on Electronics, Communications and Computers (JEC-ECC)*, Dec. 2013, pp. 135–139.

[35] F. R. Gfeller and U. Bapst, "Wireless in-house data communication via diffuse infrared radiation," *Proceedings of the IEEE*, vol. 67, no. 11, pp. 1474–1486, Nov. 1979.

[36] J. Sun, "Orthogonal frequency division multiplexing (ofdm)for wireless communication," *Wireless Communication Research Laboratory*, 2003.

[37] J.Armstrong and A.J.Lowery, "Power efficient optical ofdm," *Electron.Lett.*, vol. 42, pp. 370–372, 2006.